PDL-1+ Neutrophils mediate susceptibility during endotoxemia in Metabolically Dysfunctional-Associated Fatty Liver Disease

Cleyson da Cruz Oliveira Barros[1,2*], Alexandre Kanashiro[1,2*], Gabriel Victor Lucena da Silva[1,2], Paulo Sérgio de Almeida Augusto[1,2] , Guilherme Cesar Martelossi Cebinelli[1,2],; Luiz Osório Leiria[1,2], Thiago Mattar Cunha[1,2], José Carlos Alves Filho[1,2], and Fernando Queiroz Cunha[1,2]

[1]Center for Research in Inflammatory Diseases (CRID), Ribeirão Preto Medical School, University of São Paulo, Av. Bandeirantes; Rua das Paineiras, Casa 3, Ribeirão Preto, São Paulo, 14049-900, Brazil.

[2]Department of Pharmacology, Ribeirão Preto Medical School, University of São Paulo, Ribeirão Preto, São Paulo, Brazil.

*These authors contributed equally to this work

e-mail: fqdcunha@fmrp.usp.br

Abstract

Metabolically Dysfunctional-Associated Fatty Liver Disease (MAFLD) is a pathological condition affecting many individuals worldwide. Patients with MAFLD are more susceptible to systemic inflammation, including endotoxemia, which accelerates the progressive liver damage. However, the immunological mechanisms that trigger the hyper-inflammatory responses in individuals with MAFLD remain unknown. In the present study, we reported that short-term HFCD (Choline Deficient High Fat Diet)-fed mice, which did not show significant signs of hepatic damage and inflammation in the first two weeks, are more susceptible to a non-severe sepsis-like systemic inflammation induced by LPS challenge. Mechanistically, endotoxemic mice show an excessive accumulation of NK-producing IFN-γ cells in liver tissue, which trigger the recruitment and polarization of a distinct subset of neutrophils, characterized by high expression of PD-L1 and massive release of TNFα. Remarkably, genetic inhibition of IFN-γ or pharmacological blockade of PD-L1 effectively modulated the excessive recruitment of these neutrophils to the liver and TNF-α production, thereby preventing hepatic damage and reducing the severity of host mortality. Thus, these results support the design of novel effective strategies to control hyperinflammatory responses in septic HFCD patients and consequently improve their survival.

Key Words: neutrophil; MAFLD; endotoxemia; PDL-1.

1. INTRODUCTION

Metabolically-dysfunction-associated fatty liver disease (MAFLD), previously described as non-alcoholic fatty liver disease (MAFLD), is a metabolic liver dysfunction defined as an abnormal accumulation of fat in the liver without secondary triggers such as alcohol consumption. MAFLD has become a common chronic liver disease in the world population and has a high prevalence varying from simple steatosis to non-alcoholic steatohepatitis, fibrosis, cirrhosis, and hepatocellular carcinoma (1–3). Despite its high prevalence and increasing cause of liver-related mortality worldwide, MAFLD is still underestimated, and there are no approved pharmacological or preventive strategies for these medical conditions (4, 5).

The MAFLD is a highly complex condition that involves a “multi-hit” process, in which different stimuli act together to promote fat accumulation and progressive liver damage (6). Although the pathogenesis of MAFLD is multifactorial, inflammation has now been considered a key factor in the progression of advanced hepatic conditions (7–9). In the presence of obesity and lipotoxicity, the immune system is activated in the liver, with a corresponding degree of inflammation triggered by the “wound healing response”. Since these inflammatory signs persist for a long period, monocytes and neutrophils, as well as T CD4, T CD8, and natural killer (NK), can be recruited to the liver, releasing a massive secretion of pro-inflammatory cytokines, including interferon-gamma (IFN-γ) and tumor necrosis factor (TNFα) (7, 10). Likewise, in chronic diseases, these cytokines are also present in systemic and uncontrolled inflammatory processes, such as sepsis (11). Sepsis is a syndrome characterized by a life-threatening dysfunction due to complex interactions between pathogens and the host recruitment of immune cells, resulting in a systemic hyper-inflammatory state followed by extensive vital organ damage, including in the liver (12, 13). Sepsis has also been considered the leading cause of death in intensive care units. In endotoxemia, a well-established sepsis model, this massive production of cytokines provokes uncontrolled recruitment of innate immune cells, mainly monocytes and neutrophils, to vital organs, including the liver, where they induce extensive and lethal damage (11, 14, 15). The majority of data regarding endotoxemia pathogenesis has focused only on the interaction between the infection and the host immune system, and only a few studies have addressed one or more clinical conditions that are considered risk factors leading to endotoxemia aggravation, such as senescence and previous immunosuppressive comorbidities (16–18). Thus, understanding how these

clinical conditions can modify the host immune response and consequently affect the outcome of sepsis is crucial to detecting the risks and designing novel preventive and therapeutic approaches to control exacerbated inflammatory responses. Recently, some population studies, including large-scale data from cohorts with biopsy-confirmed individuals, have evidenced a higher incidence of severe infections in MAFLD patients~~,~~ suggesting that previous hepatic conditions can modify the host immune response, leading to sepsis aggravation (19). However, although a relationship between elevated risk of sepsis in MAFLD patients exists, the underlying immunological mechanisms involved in the progression and exacerbation of systemic and/or local (hepatic) inflammation in these individuals have not been identified yet.

To understand the impact of MAFLD on liver damage during endotoxemia, we used a known murine model of MAFLD and later challenged these animals with a moderate dose of lipopolysaccharide (LPS). We demonstrated that endotoxemia exacerbated the hepatic inflammatory response and mortality in Choline Deficient High Fat Diet (HFCD)-fed mice. The LPS-activated hepatic NK cells secrete IFN-γ, which induces massive recruitment and polarization of a specific subpopulation of PD-L1-expressing neutrophils. This subpopulation of neutrophils releases a high concentration of TNFα, which mediates the liver lesion and increases the mortality of the animals. In fact, biological treatments promoting PD-L1 neutralization, or neutrophil depletion, reduced the TNF-α concentration, the liver inflammatory response and organ pathology, and increased the survival in endotoxemic HFCD fed mice. Similar results were observed with the use of genetic knockout TNF-α receptor mice. Thus, our findings describe the potential mechanism involved in the exacerbation of neutrophil functions in MAFLD mice and suggest a viable approach to the development of individual interventions capable of mitigating the hyperinflammation observed in these pathological conditions.

2. RESULTS

MAFLD mice are more susceptible to LPS-induced systemic inflammation.

To study MAFLD as a pre-condition associated with increasing risk of exacerbation of inflammation induced by endotoxemia, we employed a murine model of MAFLD in which the mice were fed for two weeks with a choline-deficient high-fat HFCD diet, a well-known liver disease model (Fig. 1A). As a result, we used a two-week diet period during which no changes in lymphocyte numbers were observed because the HFCD, which is choline-deficient, leads to a reduction in lymphocyte numbers in the animals (20). Mice fed HFCD showed no increase in liver weight and collagen deposition as evidenced by picrosirius staining (Fig. S1A and Fig. S1C). The HFCD mice challenged with LPS (10 mg/kg; intraperitoneally triggered an elevated susceptibility with an index of mortality of 100% 24 h after the challenge (Fig. 1B). In our experimental condition, this dose of LPS provoked moderate (below 40%, 4 days after LPS challenge) mortality in chow-fed mice (control group) (Fig. 1B). Compared with the control group, the HFCD animals challenged with LPS showed elevated liver damage, evidenced by an increase in plasma alanine aminotransferase (ALT) levels (a known marker of liver injury) and histopathological alteration, characterized by leukocyte infiltration and edema (Fig 1C,1E). Compared with control mice treated with PBS, the HFCD animals also treated with PBS did not show significant signs of hepatic damage and local inflammatory response, evidenced by the absence of leukocyte infiltration (Fig. 1C and 1E). Animals subjected to the HFCD diet showed reduced blood glucose levels with or without LPS challenge (Fig. S1B). Remarkably, compared to the Chow group, HFCD mice exposed to LPS did not show greater changes in other organs commonly affected by endotoxemia, such as the kidneys (Figure 1D), indicating that a pathological inflammatory condition is increased mainly in liver tissue compared to other organs. To assess how MAFLD modulates the immune response in the hepatic microenvironment of human patients, we reanalyzed previously published bulk RNA-seq data from patients with MAFLD to identify potential targets related to the inflammatory process (21). Firstly, we performed analyses of genes differentially expressed in leukocyte samples from patients with MAFLD and healthy controls. We observed that 5240 genes are upregulated, such as *EIF4H*, *TMEM*, *MOB1A*, *SERBP1*, *TM9SF1*, *HINT3*, *ARF3*, *CHTF8*, and *PDIA6*, while 5806 genes, as *FOSB*, *KAT2A*, *SNRNP70*, *CCNL2*, *AMY2B*, *EXD3*, and *EBNA1BP2, are*

141 downregulated. Interestingly, we found that the *CD274* gene (encoding PD-L1) and
142 the *IFNGR2* gene, corresponding to the IFN-γ receptor, are among the upregulated
143 genes (Fig. 2A). Furthermore, after conducting an additional enrichment analysis of
144 the 5240 upregulated genes using Gene Ontology (GO), we detected an increase in
145 several pathways associated with inflammatory processes, such as phagocytosis,
146 leukocyte migration, immune response to bacterial components, and signaling
147 pathways involving IL-1β, TNF-α, and IFN-γ (Fig. 2B).

148 Because IFN-γ and TNF-α signaling pathways are upregulated in MAFLD
149 patients, we reanalyzed previously published single-cell RNA-seq data from liver
150 samples from mice fed with a 60% high-fat diet, another known MAFLD model (22).
151 We noticed an increase in immune cells in the hepatic tissue, such as monocytes,
152 neutrophils, dendritic cells, T cells, and NK cells (Fig. 2C and 2D). Interestingly, we
153 observed a specific upregulation of CD274 and TNF-α genes in monocytes and
154 neutrophils, while T cells and NK cells showed increased IFN-γ expression (Fig. 2E),
155 suggesting that the cytokines produced by these specific cells may be involved in the
156 hyperinflammation observed during MAFLD.

157 Next, based on the results of increased IFN-γ and TNF-α signaling in bulk
158 RNAseq and single-cell RNA sequencing analyses in hepatic samples of MAFLD
159 patients and animals, we investigated the role of these cytokines in the susceptibility
160 of endotoxemic MAFLD mice. Initially, we observed an exacerbated hepatic production
161 of both cytokines induced by endotoxin challenge in the HFCD-fed group compared to
162 the control mice treated with PBS or LPS (Fig. 3A and 3B). Furthermore, we also
163 observed that IFN-$\gamma^{-/-}$ and TNFR1R2$\alpha^{-/-}$ mice with MAFLD challenged with LPS did not
164 show an increase in the enzyme ALT, a liver lesion marker (Fig. 3C and 3D). In
165 addition, endotoxemic MAFLD TNFR1R2$^{-/-}$ and IFN-$\gamma^{-/-}$ mice exhibited reduced
166 leukocyte infiltration in the liver tissue and improved survival (Fig. 3E, 3F, and 3G),
167 respectively, as compared to endotoxemic WT mice. Furthermore, splenocytes from
168 HFCD-fed IFN-deficient animals exhibited increased IL-6 and TNF-α production upon
169 *in vitro* LPS stimulation, indicating a response pattern similar to that of control animals
170 (Fig 2SA and Fig. 2SB). Together, our data demonstrate that MAFLD predisposes to
171 the exacerbation of cytokine production, such as IFN-γ and TNF-α, which mediate an
172 elevated index of mortality in endotoxemic mice.
173

174 **MAFLD induces the recruitment of NK cells that are sources of IFN-γ**
175 **production in endotoxemia**

176 During the inflammatory process, it is already established that CD4 and CD8 T
177 cells are important sources of IFN-γ(23). Herein, we observed a selective increase in
178 IFN-γ production by CD8, but not CD4, T cells during endotoxemia (Fig. 4A, Fig. 4B,
179 Fig. S3A, Fig. S3B), respectively. In light of this, we next investigated the involvement
180 of lymphoid cells in the high susceptibility of endotoxemic mice with MAFLD. For this,
181 we submitted animals with the absence of T and B cells (*Rag1*$^{-/-}$ mice) to the MAFLD
182 protocol, and after challenging them with LPS and the survival rate was assessed.
183 Interestingly, *Rag1*-deficient animals under the HFCD remained susceptible to the
184 LPS challenge (Fig. 4C) with exacerbation of liver injury (Fig. 4D), suggesting that
185 these T and B cells do not contribute to susceptibility to the LPS challenge.

186 Recent studies have demonstrated that NK cells are other IFN-γ-producing
187 cells recruited to the hepatic tissue during MAFLD and that they are also involved in
188 systemic inflammatory responses, including sepsis (24–29). We observed that the
189 number of NK cells increased in the liver tissue of PBS-treated MAFLD mice compared
190 with HFCD fed a control diet (Fig. 4E). LPS challenge increased the accumulation of
191 NK1.1+CD3− NK cells in the liver tissue of MAFLD mice and the absence of
192 NK1.1+CD3+ NKT cells (Fig. S3C and 4E). Furthermore, our cytometric analyses
193 demonstrated that NK cells infiltrated in the liver tissue secrete high levels of IFN-γ
194 (Fig.S3D and 4F). Next, to confirm the pathological involvement of NK cells during
195 hyperinflammation in MAFLD, we depleted these cells by treating animals with anti-
196 NK antibody 1.1, one day before the LPS challenge (Fig. S4). Interestingly, the
197 pharmacological depletion of NK cells in MAFLD animals provoked an increased
198 survival index (Fig. 4G). Furthermore, when NK cells were depleted, MAFLD animals
199 exhibited reduced hepatic damage (Fig. 4H), IFN-γ levels (Fig. 4I), and TNF-α levels
200 (Fig.4J). Together, these results suggest that NK cells are responsible for susceptibility
201 via IFN-γ production in MAFLD during endotoxemia.

202

203 **Neutrophils are responsible for susceptibility during hyperinflammation**
204 **in MAFLD**

205 During MAFLD development, innate immune cells, such as monocytes and
206 neutrophils, are the first leukocytes recruited to the liver (24, 30). With this in mind,
207 mice with MAFLD were challenged with LPS, and the infiltration of these cells in the

208 liver was quantified. During the initial inflammatory phase, six hours after the LPS
209 challenge, we observed that monocytes were recruited to the site (Fig. 5A and 5B).
210 Since inflammatory monocytes emigrate from the bone marrow towards the periphery
211 via CCR2 and then migrate to inflamed tissues, differentiating into monocyte-derived
212 macrophages (30, 31), we investigated the functional role of monocytes in MAFLD,
213 using CCR2-deficient mice (Fig. 5S). Interestingly, animals deficient in monocyte
214 migration (CCR2-/-) showed a high mortality rate compared to wild type after LPS
215 challenge and neutrophil migration was not altered (Fig. 5SA and Fig. 5SB). Moreover,
216 CCR2-/- animals subjected to the respective diets had leukocyte CD45+ infiltration
217 similar to that observed in the LPS challenge control mice (Fig. 5SC and Fig. 5SD).
218 Furthermore, the survival rate of MAFLD CCR2-/- mice challenged with LPS was not
219 different of MAFLD wild type mice also challenged with LPS (Fig. 5SB). Together, the
220 results suggest that monocytes do not contribute to susceptibility in endotoxemic
221 animals with MAFLD
222 In addition to monocytes, granulocytes are innate immune cells recruited to the
223 hepatic tissue during the development of MAFLD (19). We observed that high levels
224 of neutrophils are present in the hepatic tissue of animals with MAFLD and that their
225 recruitment is exacerbated in the hepatic microenvironment in endotoxemic mice (Fig.
226 5A and 5C). It is known that neutrophils are recruited to the inflammatory focus via
227 CXCR2 (32). To understand the involvement of these receptors and neutrophils in
228 MAFLD during endotoxemia, MAFLD animals were pre-treated one day before the
229 LPS challenge with CXCR2i or with anti-Ly6G, which depletes these cells throughout
230 the organism. Interestingly, after both treatments, we observed a reduction of the
231 leukocyte infiltration into the hepatic tissue (Fig. 5D) and a decrease in hepatic lesions
232 (ALT) (Fig. 5E) and TNF-α levels (Fig. 5F). Confirming the participation of granulocytes
233 in susceptibility after the LPS challenge in MAFLD, animals treated with CXCR2i and
234 anti-Ly6G showed an improvement in their survival (Fig. 5G and 5H).
235
236 **IFN-γ induces CD274 expression during endotoxemia in animals with**
237 **MAFLD**
238 IFN-γ is a cytokine that plays a crucial role in the T and NK cell-mediated
239 immune response (27–29, 33–35). Recent studies have shown that this inflammatory
240 cytokine also induces the expression of checkpoint molecules, such as programmed
241 death-ligand 1 (PD-L1), in different immune cells, including neutrophils (30, 36, 37).

242 Analyzing datasets from mice with MAFLD, we observed the upregulation of the
243 CD274 (PD-L1) gene and TNF-α in neutrophils and IFN-γ in NK cells (Fig. 1C, Fig1D,
244 and Fig. 1E). Considering these findings, we investigated whether IFN-γ induces the
245 expression of PD-L1 in neutrophils in MAFLD mice during endotoxemia. First, we
246 observed that only the MAFLD diet caused a significant increase in PD-L1 expression
247 in CD45+CD11b+ leukocytes after LPS challenge (Fig. S6C). We observed that within
248 this population, neutrophils predominate in their expression when compared to
249 monocytes (Fig. 6SA-6SD). Furthermore, PD-L+1 neutrophils showed an exacerbated
250 migration of PD-L1+ neutrophils towards the liver (Fig. 6A and 6B). Next, to confirm
251 the role of IFN-γ in the expression of PD-L1, we investigated whether IFN-γ is capable
252 of increasing the expression of PD-L1 in neutrophils after the LPS challenge of
253 MAFLD. Mice with MAFLD lacking IFN-γ were challenged with LPS and assessed for
254 PD-L1 expression in granulocytes. Interestingly, in the absence of IFN-γ, neutrophils
255 do not express PD-L1, and their infiltration in the liver was attenuated (Fig. 6C and
256 6D).

257 As demonstrated previously in sepsis, PD-L1 neutrophils showed reduced rates
258 of apoptosis (36). Therefore, we cultured neutrophils in the presence of IFN-γ and/or
259 LPS and assessed their apoptosis rate. Interestingly, in these *in vitro* conditions,
260 neutrophils expressing PD-L1 showed reduced rates of apoptosis (Fig. 6E and 6F),
261 suggesting that PD-L1-expressing neutrophils can survive for long periods in the
262 hepatic environment in MAFLD, accentuating the LPS-induced inflammatory
263 response.

264

265 **Neutrophils expressing PD-L1+ secrete TNF-α during hyperinflammation**
266 **in MAFLD**

267 There is also evidence that excessive secretion of TNF-α by immune cells,
268 especially neutrophils, may be associated with liver damage and the progression of
269 MAFLD (36, 37). To investigate a possible link between the expression of PD-L1 by
270 the neutrophils and their ability to express TNF-α, mice undergoing MAFLD were
271 exposed to LPS, and the expression of TNF-α by PD-L1+ neutrophils was assessed.
272 We observed an exacerbated expression of TNF-α by PD-L1+ neutrophils from
273 MAFLD when compared to control animals (Fig. 7A, Fig. 7B, Fig. 7D and Fig8SG) and
274 no increase in TNF-α^{+}PDL1^{-} neutrophils (Fig. 7C). These results illustrate that after
275 exposure of MAFLD animals to LPS, the expression of PD-L1 by neutrophils is linked

276 to heightened TNF-α expression compared to control animals fed standard chow. To
277 assess whether the lack of TNF-α signaling immunomodulates the granulocytic
278 recruitment to the liver tissues in MAFLD animals, TNF receptor R1 and R2 knockout
279 animals (TNF R1R2) were exposed to LPS. It was also observed that the absence of
280 TNF-α did not interfere with the recruitment of neutrophils to the liver tissue (Fig. S8A
281 and Fig. S8C) or the expression of PD-L1 in neutrophils (Fig. S8B and Fig. S8D).
282 Similarly, the absence of TNF-α receptors in MAFLD during the challenge with LPS
283 did not interfere with the production of IL-10 and IFN-γ (Fig. S8E and Fig. S8F).
284 However, as described above, the absence of the TNF R1R2 receptor reduced liver
285 injury and mortality induced by LPS administration in MAFLD (Fig. 3D and Fig. 3F).
286 Considering that NK cells present in liver tissue secrete IFN-γ (Fig. 4E) and that
287 in IFN-$\gamma^{-/-}$ animals, there is a reduction in TNF-α levels in the liver of mice with MAFLD
288 during endotoxemia (Fig. 4K), we next examined whether PD-L1+TNFα+ neutrophils
289 are present in MAFLD animals depleted of NK cells. It was observed that in the
290 absence of NK cells, PD-L1+TNFα+ neutrophils were not detected (Fig. 7E, Fig. 7F,
291 and Fig. 7G), confirming that IFN-γ secreted by NK cells is crucial for inducing PD-L1
292 expression and TNF-α secretion by neutrophils in the hepatic tissue in MAFLD animals
293 after LPS administration.
294
295 **Anti-PD-L1 treatment protects animals with MAFLD during**
296 **hyperinflammation**
297 Next, we investigated the potential role of PD-L1 in TNF-α production by
298 neutrophils and in the lesions in MAFLD mice. Initially, we found that anti-PD-L1, a
299 biological drug inhibiting PD-L1's interaction with PD-1, effectively prevented liver
300 inflammation and tissue damage (Fig. 8A, Fig. 8B, and Fig. 8F). Additionally, this
301 treatment reduced liver TNF-α levels without affecting IFN-γ (Fig. 8C) and improved
302 host survival (Fig. 8D). Importantly, anti-PD-L1 did not decrease the number of
303 recruited NK cells in all groups studied (Fig. 8I and Fig. 8L). Notably, treatment with
304 anti-PD-L1 successfully blocked LPS-induced neutrophil recruitment and the
305 increased presence of PD-L1-expressing neutrophils in mice on HFCD (Fig. 8J and
306 Fig. 8K), while these parameters remained unchanged in mice fed a standard chow
307 diet (Fig8G, Fig8H). Overall, our findings suggest that anti-PD-L1 therapy primarily
308 suppresses exaggerated TNF-α production by neutrophils in MAFLD mice without
309 affecting the IFN-γ secretory activity of NK cells mechanistically.

310
311
312 ## 3. DISCUSSION

313 The pathogenesis of MAFLD and sepsis had been considered two independent
314 conditions, associated with local and systemic inflammatory response, respectively.
315 MAFLD is a chronic liver dysfunction characterized by the buildup of fat in the liver in
316 individuals who do not consume excessive amounts of alcohol. On the other hand,
317 sepsis is an inflammatory state triggered by an infection that leads to damage to vital
318 organs, including the lungs and liver. This occurs when the body's immune response
319 fails to contain the microorganisms at the site of the primary infection(9). Recent
320 studies demonstrate that the presence of MAFLD is associated with an increased risk
321 of developing sepsis (38, 39), but the exact mechanisms underlying this association
322 are not fully understood. In the present study, we observed that MAFLD mice induced
323 by an HFDC diet are more susceptible to a systemic and hepatic hyper-inflammatory
324 state induced by endotoxemia, confirming in our experimental condition that MAFLD
325 can be considered a crucial risk factor of sepsis progression, even when MAFLD or
326 hepatic inflammation is not yet detected. The LPS administration promotes the
327 polarization of a specific subset of granulocytes expressing PD-L1, which secrete high
328 levels of TNF-α in an NK-derived IFN-γ dependent manner. The released TNF-α plays
329 an important role in the liver lesion. We also observed that CD4+ and CD8+ T cells or
330 monocyte cells do not seem to participate in the mice's susceptibility in this hyper-
331 inflammatory state. In accordance, previous studies implicated NK cells in liver injuries
332 in different MAFLD and sepsis experimental models(25, 40–44). It was observed that
333 during severe sepsis, NK cell-released IFN-γ play a detrimental role in mediating
334 tissue injury (44). Similarly, in MAFLD, NK cells can accumulate in the liver and release
335 IFN-γ, which contributes to the development of hepatic inflammation and fibrosis(45).
336 Therefore, these studies, support that the increase in NK cells induced by
337 endotoxemia in MAFLD animals, along with IFN-γ secretion, appears to have a crucial
338 role in the increased susceptibility of these pathological conditions, contributing to
339 disease progression.

340 Considering this evidence, we re-analyzed previously published bioinformatic
341 data (21, 22) and observed that, in MAFLD patients, IFN-γ and TNF-α are up-
342 regulated, and that, in high-fat high fructose diet-fed mice, there is up-regulation of
343 IFN-γ in NK cells, and TNF-α and CD274 (PD-L1) in myeloid cells (21, 22), suggesting

344 that similar immune dysfunctions are observed in patients and experimental models
345 of MAFLD. To add experimental information about how the IFN-γ mediates the liver
346 lesion, we demonstrated that in endotoxemic MAFLD animals hepatic neutrophils are
347 important producers of TNFα, and this release is stimulated by NK-derived IFN-γ
348 signaling. In addition, IFN-γ promoted the differentiation of PDL-1-expressing
349 neutrophils, given that in those animals depleted of NK, the neutrophils did not exhibit
350 this activated phenotype. Moreover, the PDL-1-expressing neutrophils showed a
351 reduced apoptosis rate, increasing the retention time of the neutrophils in hepatic
352 tissue. Thus, these events could explain the increase in hepatic injury in MAFLD
353 animals during endotoxemia. According, in the context of infection-triggered
354 inflammation, the participation of IFN-γ in modulating neutrophil pro-inflammatory
355 profiles, including the expression of PD-L1, has been demonstrated (36). Neutrophils,
356 as frontline innate immune cells, control pathogens through phagocytosis and the
357 release of microbial mediators, including cytokines, cytosolic enzymes, free radicals,
358 and NETs (46, 47). However, excessive neutrophil activity can lead to tissue damage,
359 particularly in sepsis, where they contribute significantly to multi-organ damage via the
360 overproduction of inflammatory mediators, including TNF-α (16, 48, 49). Our data
361 demonstrate that during MAFLD, liver neutrophils are major sources of TNF-α
362 production induced by endotoxemia. Confirming the involvement of TNF-α release by
363 PDL-1+ neutrophils stimulated by NK cells-derived IFN-γ in the increase of
364 susceptibility of MAFLD, we demonstrated that the absence of TNF-α signaling or
365 depleted NK cells led to improved survival in mice with MAFLD during endotoxemia.
366 However, the absence of TNF-α signaling did not affect PD-L1 expression in
367 neutrophils. These findings imply that, while TNF-α plays a crucial tissue lesions, its
368 intracellular signaling does not notably impair the expression of PD-L1 in the
369 neutrophils or their migration into liver tissue during MAFLD. To reinforce that
370 neutrophils are the main source of the TNF-α involved in susceptibility of MAFLD by
371 endotoxemia, we evaluate whether the neutralization of these cells with specific
372 antibodies could improve the survival of endotoxemic HFDC-fed mice. Numerous
373 strategies for targeting neutrophils are being investigated in various clinical and
374 experimental settings (12, 50), including the use of CXCR2 inhibitors in patients with
375 NASH (13, 50). Interestingly, we demonstrated that targeting neutrophils with different
376 biological drugs, similar to the inhibition of TNF-α, mitigated inflammation-induced liver
377 lesions.

378 Recent studies suggest that during the progression of MAFLD, PD-L1 is
379 expressed in both parenchymal and non-parenchymal cells (10, 51). Given that the
380 neutrophils responsible for hepatic damage in endotoxemic MAFLD mice exhibit a
381 specific PD-L1-expressing phenotype, *we* demonstrated that anti-PD-L1 significantly
382 reduced TNF-α-producing PD-L1+ neutrophils in the liver environment, attenuating
383 endotoxemia-induced inflammation and liver damage, ultimately reducing mortality in
384 MAFLD mice. This highlights the role of PD-L1 expression in neutrophils in promoting
385 a proinflammatory phenotype associated with heightened TNF-α production and
386 susceptibility of endotoxemic HFDC-fed mice. In the context of endotoxemia, recent
387 research indicates that PD-L1-expressing neutrophils also contribute to
388 immunosuppression and increased susceptibility to secondary infections (52) and also
389 contribute to lung injury. Thus, our data support that the inhibition of PD-L1, besides
390 preventing the organ lesions induced by sepsis in MAFLD patients, could also prevent
391 the long-term immunosuppression observed in these patients.

392 Although macrophages, including Kupffer cells, have been considered a
393 relevant source of cytokines in endotoxemic animals (53, 54), we did not find an
394 important role for these cells expressing CCR2 in the aggravation of endotoxemia,
395 since the absence of these chemokine receptor, which governs the migration and
396 differentiation of inflammatory monocytes into macrophages, did not influence the
397 endotoxemia mortality in animals with MAFLD. However, it's worth noting that we did
398 not extensively investigate the interaction of IFN-γ and TNF-α in the role of monocytes
399 in our model, necessitating further studies to unravel the possible mechanisms of
400 these cells.

401 Our study presents several limitations that should be acknowledged and
402 discussed. First, we cannot entirely rule out the possibility that our mice deficient in
403 pro-inflammatory components exhibit reduced responsiveness to LPS. However, our
404 ex vivo analyses using splenocytes from these animals revealed a preserved cytokine
405 production following LPS stimulation. These results suggest that the in vivo differences
406 observed are primarily driven by the MAFLD condition rather than by intrinsic defects
407 in LPS sensitivity. Second, the absence of publicly available single-cell RNA-seq
408 datasets from MAFLD subjects under endotoxemic or septic conditions limited our
409 ability to perform direct translational comparisons. To overcome this, we analyzed
410 existing MAFLD patients and experimental MAFLD datasets, which consistently
411 demonstrated upregulation of IFN-γ and TNF-α inflammatory pathways in MALFD. In

line with these findings, our murine model revealed TNF-α$^+$ myeloid and IFN-y$^+$ NK cell populations, thereby reinforcing the validity and translational relevance of our results.

Overall, our findings establish a biological basis for understanding the progression of endotoxemia in MAFLD, highlighting the dysregulated role of neutrophils in which hepatic metabolic syndrome potentiates the inflammatory effects of granulocytes via NK cells, advocating interventions to mitigate this inflammatory condition.

446

447 ## 4. MATERIAL AND METHODS

448 ### Experimental Design

449 This study was designed to interrogate the pathologic mechanisms in MAFLD
450 during endotoxemia-induced generalized inflammation. The mice were submitted to
451 the HFDC diet for two weeks, and subsequently, LPS administration and the cellular
452 mechanisms were outlined after 6h of the challenge, knowing that no animal
453 succumbed to death (indicated by survival). Furthermore, knockout animals and those
454 treated with pharmacological inhibitors or neutralizing antibodies shared the same
455 control groups (chow and HFCD), as required by the animal ethics committee.
456 Inflammatory infiltrates along with liver lesions were assessed based on H&E-stained
457 tissue sections, and endpoint analyses included flow cytometry.

458

459 ### Animals

460 The mice used in this study were in the C57BL/6 genetic background and
461 included CCR2 $^{-/-}$, IFN-γ$^{-/-}$, and TNFR1R2 $^{-/-}$. Male mice aged 5 to 6 weeks were reared
462 and maintained under specific pathogen-free conditions in the University of São Paulo
463 vivarium, FMRP/USP. All animals received food and water ad libitum, at 25°C, with
464 food and water ad libitum. Mice were fed a standard low-fat diet (hereinafter referred
465 to as the standard "Chow" diet – 10% of calories derived from fat) or a Choline
466 Deficient High Fat Diet (referred to as "HFCD", 60% of calories derived from fat and
467 choline-deficient) for 2 weeks for the development of MAFLD. The diets were provided
468 by Rhoster (Araçoiaba da Serra- São Paulo). Care for the mice complied with
469 institutional guidelines on ethics in animal experiments; approved by CETEA (Ethics
470 Committee for Animal Experimentation of the Faculty of Medicine of Ribeirão Preto,
471 approved protocol number 193/2019).

472

473 ### Endotoxemia

474 Lipopolysaccharide (LPS; Escherichia coli (O111:B4), L2630, Sigma-Aldrich,
475 St. Louis, MO, USA) was administered intraperitoneally (i.p.; 10 mg/kg) in C57BL/6,
476 CCR2 -/-, IFN-γ-/-, and TNFR1R2 -/- mice. The HFCD was initiated in 5–6 week-old
477 mice, and LPS was administered after 2 weeks on the diet, meaning that LPS
478 administration occurred when the mice were 7–8 weeks old, with body weights ranging

479 from 22 to 26 g. LPS was previously solubilized in sterile saline and frozen at -70°C.
480 The animals were euthanized 6 hours after LPS administration.
481
482 **Hepatic non-parenchymal cell isolation**
483 Livers were collected, and 200-300 mg of tissue was taken for flow cytometry
484 analysis. The tissue was minced with surgical scissors and then digested with 1 mg of
485 collagenase II, and 60 U/ml of DNase I in PBS at 37 °C for 45 minutes, shaking at 110
486 rpm. The digested tissue was then processed through a 100 µm cell strainer and
487 centrifuged at 1,500 rpm for 5 minutes. Subsequently, the isolation of non-
488 parenchymal cells was performed by Percoll (GE Healthcare) centrifuged at 2300rpm
489 at 22 °C for 30 minutes, subjected to ACK (red blood cell lysis), and resuspended in
490 0.5% BSA in PBS for staining. Single-cell suspensions were stained with Zombie Aqua
491 viability stain (Biolegend), blocked with TruStain FcX (Biolegend), and then stained
492 with flow cytometry antibodies when indicated; antibodies are tabulated in Table S1.
493 As animals were already in a hyperinflammatory state, no additional in vitro stimulation
494 was required. Intracellular detection of IFN-γ and TNF-α was conducted using the
495 Foxp3 staining kit (eBioscience). Since both antibodies were conjugated to PE,
496 staining and analyses were performed in separate experiments. Cells were collected
497 on the CANTO II flow cytometer using BD FACS Diva software and then analyzed
498 using FlowJo (USA).
499
500 **Histology**
501 Mouse livers were fixed in 10% formalin overnight, washed twice with PBS, and
502 placed in 70% ethanol or PBS until processing. For H&E, tissues were embedded in
503 paraffin, sectioned, and stained with H&E at the MGH Histopathology Research Core.
504
505 **Cytokine quantification**
506 For the detection of IFN-γ, TNF-α, and IL-10 in the liver, tissue samples were
507 weighed and titrated in 1 mL of PBS Complete (Roche Diagnostics, Mannheim,
508 Germany) containing a cocktail of protease inhibitors. Cytokine levels were determined
509 using commercial ELISA kits for IFN-γ, TNF-α, and IL-10 (Biolegend, USA).
510 Wavelength correction and background signals were subtracted from absorbance
511 values
512

513 **Serum analysis**

514 At the time of sacrifice, blood samples were collected in EDTA collection tubes
515 and subsequently centrifuged to obtain serum. Serum ALT and Urea levels were
516 measured using a colorimetric kit (BioQuant, Heidelberg, Germany) according to the
517 manufacturer's instructions.

518

519 **Neutrophil targeting**

520 For neutrophil targeting, antibodies/inhibitors were used as follows: Anti-Ly6G
521 (BioXCell, catalog # BP0075) was administered at 500 mg/kg per mouse on day 13
522 after starting the diet (24h before inoculation of the LPS) and sacrificed on day 14. For
523 survival studies, all mAbs were inoculated once daily for 7 days. CXCR2 inhibitor SB
524 225002 (Tocris, catalog #2725/10) was injected at 200 mg per dose and programmed
525 as anti-Ly6G. For anti–PD–L1–based neutrophil targeting, anti–PD-L1 (BioXCell,
526 catalog #BE0101) was injected at 12.5 mg/kg ~12h before the LPS challenge and
527 again 1 day after treatment, each time followed by anti-mouse IgG2b (12.5 mg/kg)
528 (BioXCell, catalog no. BE0252). All injections were intraperitoneal.

529

530 **Neutrophil purification and apoptosis assay**

531 Peripheral blood samples were collected by venipuncture and centrifuged at
532 450 × g for plasma separation. The blood cells were then resuspended in Hank's
533 balanced salt solution (Corning; cat. 21-022-CV), and the neutrophil population was
534 isolated by Percoll density gradient (GE Healthcare; cat. 17-5445-01) (72 %, 63%,
535 54% and 45%). Isolated neutrophils were resuspended in RPMI1640 (Corning; cat.
536 15-040-CVR) supplemented with 0.5% BSA. Neutrophil purity > 95% was determined
537 by Rosenfeld color Cytospin (Laborclin; cat 620529)

538 To quantify apoptosis, cells were permeabilized with Triton X-100 and stained
539 with propidium iodide. After 10 minutes of incubation at 4 degrees in the dark,
540 neutrophil apoptosis was quantified as PI+ staining on FACSCanto II (Becton
541 Dickinson, Franklin Lakes, NJ, USA). Results were analyzed using Flowjo software
542 (Tree Star, Ashland, OR, USA). Apoptosis was detected as a measure of the
543 hypodiploid peak in PI fluorescence histograms, as described by Nicoletti et al. BD
544 Bioscience, Franklin Lakes, NJ, USA) and Annexin V and 7-AAD double staining
545 (Biolegend, San Diego, USA).

546

547 **Splenocyte culture**

548 Mice were fed a control chow or HFCD diet for 2 weeks. Animals were
549 euthanized, and spleens were aseptically removed in cold PBS (Gibco) and then
550 mechanically dissociated through a 100-µm cell strainer to obtain a single-cell
551 suspension. Red blood cells are lysed with ACK buffer for 1–2 min at room
552 temperature, the reaction is quenched with complete RPMI 1640 medium
553 (supplemented with 10% heat-inactivated FBS, 2 mM L-glutamine, and antibiotics),
554 and cells are centrifuged and resuspended at the desired density, 1×10^6 cells/mL.
555 Splenocytes are plated in 96-well plates and incubated at 37°C, 5% CO_2. To induce
556 immune activation, cells are stimulated with lipopolysaccharide (E. coli O111:B4) at
557 concentrations ranging from 100 ng/mL to 1 µg/mL for 24 h, and cytokine dosage was
558 performed for IL-6 and TNFα.

559

560 **NK cell depletion**

561 For in vivo NK cell depletion, male C57BL/6 mice received NK cell neutralizing
562 antibody (BioXCell, catalog # PK136) or isotype-matched mouse IgG2α monoclonal
563 antibody control (BioXCell, catalog # BE0252) by intraperitoneal injection (150 µg in
564 200 µL PBS 24h before LPS challenge). To assess survival, the antibodies were
565 inoculated 24 hours before the LPS challenge and then once a day for 7 days.

566

567 **Single-cell RNA sequencing analysis**

568 We re-analyzed single-cell transcriptomic data (GSE166504) from the mouse
569 liver from mice with MAFLD and their respective control groups (21). The dataset was
570 downloaded, and the RDS file was imported into R (55) environment version v4.2.3
571 and Seurat v4.1.1 (56) by filtering genes expressed in at least 300 cells. For the pre-
572 processing step, outlier cells were filtered out based on three metrics (library size <
573 20,000, number of expressed genes between 200 and 4,000, and mitochondrial
574 percentage expression < 0,8). The top 3,000 variable genes were then identified using
575 the 'best' method using the FindVariableFeatures function. Percent of mitochondrial
576 genes was regressed out in the scaling step, and Principal Component Analysis (PCA)
577 was performed using the top 3,000 variable genes, and the top 30 PCs were selected
578 for dimension reduction by Uniform Manifold Approximation and Projection (UMAP).
579 Clusters were identified using the author's annotation. Then, differential gene
580 expression analysis was performed using the FindAllMarkers function in Seurat with

581 default parameters to obtain a list of significant gene markers for each cluster of cells.
582 Visualization of genes illustrating expression levels was performed using R/Seurat
583 commands (DimPlot, FeaturePlot, and DotPlot) using ggplot2 (57) and customized
584 (58) R packages.
585
586 **RNA sequencing analysis**
587 RNA-seq data were obtained from GSE185051 (59). The R/Bioconductor
588 package edgeR was used to identify differentially expressed genes among the
589 samples, after removing absent features (zero counts in more than 75% of samples)
590 (60). Genes with a fold change of >0.5 were identified as differentially expressed.
591
592 **Pathway enrichment analysis**
593 The list of differentially expressed genes was enriched using the ClusterProfiler
594 R package (8). Gene ontology (GO) terms in the Biological Processes category with
595 $P < 0.05$ were considered significant. Statistically significant, non-redundant GO-
596 enriched terms were plotted.
597
598 **Statistics**
599 Statistical significance was determined by two-tailed paired or unpaired
600 Student's t-test or one-way ANOVA followed by Tukey's post hoc test. Absolute
601 numbers and percentages were compared using Fisher's exact test. Spearman rank
602 order correlation (r) was calculated to describe the correlations. $P<0.05$ was
603 considered statistically significant. Statistical analyses and graphics were performed
604 using the GraphPad Prism 8.4.2 software.
605
606
607 **Author contributions:** CCOB, AK, and FQC designed the study. CCOB, AK, PSAA
608 and GCMC performed the mouse experiments. CCOB, AK, and FQC wrote the
609 manuscript. GVLS performed the bioinformatic analysis. CCOB, AK, LOL, TMC,
610 JCFAF, and FQC reviewed the manuscript.
611
612 **Competing interests**
613 The authors declare no competing interests.

Funding

Funding The research received funding from S~ ao Paulo Research Foundation (FAPESP, 2009/54014-7, 2011/19670, 2012/10438-0 and 2013/08216-2, Center for Research in Inflammatory Diseases), Coodernação de Aperfeiçoamento de Pessoal de Nivel Superior (CAPES) and Conselho Nacional de Desenvolvimento Científico e Tecnológico (CNPq)

Acknowledgements

We thank members of Group FQC for their advice and clinical assistance; and Marcella, Sergio R. Rosa, Katia Santos, Ieda Schivo for technical assistance.

References

1. Younossi ZM, et al. Global epidemiology of nonalcoholic fatty liver disease—Meta-analytic assessment of prevalence, incidence, and outcomes. *Hepatology*. 2016;64(1):73–84.

2. Younossi Z, et al. Global burden of MAFLD and NASH: trends, predictions, risk factors and prevention. *Nature Reviews Gastroenterology & Hepatology 2017 15:1*. 2017;15(1):11–20.

3. Paik JM, et al. Changes in the Global Burden of Chronic Liver Diseases From 2012 to 2017: The Growing Impact of MAFLD. *Hepatology*. 2020;72(5):1605–1616.

4. Estes C, et al. Modeling the epidemic of nonalcoholic fatty liver disease demonstrates an exponential increase in burden of disease. *Hepatology*. 2018;67(1):123–133.

5. Wong RJ, Cheung R, Ahmed A. Nonalcoholic Steatohepatitis Is the Most Rapidly Growing Indication for Liver Transplantation in Patients With Hepatocellular Carcinoma in the U.S. [published online ahead of print: 2014]. https://doi.org/10.1002/hep.26986.

6. Schuster S, et al. Triggering and resolution of inflammation in NASH [preprint]. *Nat Rev Gastroenterol Hepatol*. 2018;15(6):349–364.

7. Peiseler M, Tacke F. Inflammatory Mechanisms Underlying Nonalcoholic Steatohepatitis and the Transition to Hepatocellular Carcinoma. *Cancers (Basel)*. 2021;13(4):1–26.

8. Carpino G, et al. Increased Liver Localization of Lipopolysaccharides in Human and Experimental MAFLD. *Hepatology*. 2020;72(2):470–485.

9. Ferro D, et al. New Insights into the Pathogenesis of Non-Alcoholic Fatty Liver Disease: Gut-Derived Lipopolysaccharides and Oxidative Stress. [published online ahead of print: 2020]. https://doi.org/10.3390/nu12092762.

652 10. Lombardi R, et al. PD-1/PD-L1 Immuno-Mediated Therapy in MAFLD:
653 Advantages and Obstacles in the Treatment of Advanced Disease. *Int J Mol*
654 *Sci*. 2022;23(5). https://doi.org/10.3390/IJMS23052707.

655 11. Smith SR, et al. The cooperative effects of TNF-alpha and IFN-gamma are
656 determining factors in the ability of IL-10 to protect mice from lethal
657 endotoxemia. *J Leukoc Biol*. 1994;55(6):711–718.

658 12. Abe T, et al. Epidemiology of sepsis and septic shock in intensive care
659 units between sepsis-2 and sepsis-3 populations: sepsis prognostication in
660 intensive care unit and emergency room (SPICE-ICU). *J Intensive Care*.
661 2020;8(1):1–9.

662 13. Sakr Y, et al. Open Forum Infectious Diseases Open Forum Infectious
663 Diseases ® Sepsis in Intensive Care Unit Patients: Worldwide Data From the
664 Intensive Care over Nations Audit. https://doi.org/10.1093/ofid/ofy313.

665 14. Mcdonald B, Kubes P. Neutrophils and intravascular immunity in the liver
666 during infection and sterile inflammation. *Toxicol Pathol*. 2012;40(2):157–165.

667 15. Jenne CN, Kubes P. Immune surveillance by the liver. *Nat Immunol*.
668 2013;14(10):996–1006.

669 16. Michels EHA, et al. Association between age and the host response in
670 critically ill patients with sepsis. *Crit Care*. 2022;26(1).
671 https://doi.org/10.1186/S13054-022-04266-9/FIGURES/5.

672 17. Bouza C, López-Cuadrado T. Epidemiology and Trends of Sepsis in Young
673 Adults Aged 20-44 Years: A Nationwide Population-Based Study. *J Clin Med*.
674 2019;9(1). https://doi.org/10.3390/JCM9010077.

675 18. Knoop ST, et al. Epidemiology and impact on all-cause mortality of sepsis
676 in Norwegian hospitals: A national retrospective study. *PLoS One*.
677 2017;12(11). https://doi.org/10.1371/JOURNAL.PONE.0187990.

678 19. Ebrahimi F, et al. Risk of Severe Infection in Patients With Biopsy-proven
679 Nonalcoholic Fatty Liver Disease – A Population-based Cohort Study. *Clinical*
680 *Gastroenterology and Hepatology*. 2023;21(13):3346-3355.e19.

681 20. Raubenheimer PJ, Nyirenda MJ, Walker BR. A Choline-Deficient Diet
682 Exacerbates Fatty Liver but Attenuates Insulin Resistance and Glucose
683 Intolerance in Mice Fed a High-Fat Diet. *Diabetes*. 2006;55(7):2015–2020.

684 21. Yao K, et al. Transcriptomic profiling of a multiethnic pediatric MAFLD
685 cohort reveals genes and pathways associated with disease. *Hepatol*
686 *Commun*. 2022;6(7):1598–1610.

687 22. Su Q, et al. Single-cell RNA transcriptome landscape of hepatocytes and
688 non-parenchymal cells in healthy and MAFLD mouse liver. *iScience*.
689 2021;24(11). https://doi.org/10.1016/J.ISCI.2021.103233.

690 23. Burke JD, Young HA. IFN-γ: A cytokine at the right time, is in the right
691 place. *Semin Immunol*. 2019;43. https://doi.org/10.1016/J.SMIM.2019.05.002.

692 24. Amer J, et al. Insulin signaling as a potential natural killer cell checkpoint in
693 fatty liver disease. *Hepatol Commun*. 2018;2(3):285–298.

694 25. Martínez-Chantar ML, Delgado TC, Beraza N. Revisiting the Role of
695 Natural Killer Cells in Non-Alcoholic Fatty Liver Disease. *Front Immunol*.
696 2021;12:640869.

697 26. Wang F, et al. Activated Natural Killer Cell Promotes Nonalcoholic
698 Steatohepatitis Through Mediating JAK/STAT Pathway. *Cell Mol Gastroenterol*
699 *Hepatol*. 2022;13(1):257.

700 27. He H, et al. NK cells promote neutrophil recruitment in the brain during
701 sepsis-induced neuroinflammation. *Sci Rep*. 2016;6.
702 https://doi.org/10.1038/SREP27711.

703 28. Jensen IJ, et al. Polymicrobial sepsis influences NK-cell-mediated
704 immunity by diminishing NK-cell-intrinsic receptor-mediated effector responses
705 to viral ligands or infections. *PLoS Pathog*. 2018;14(10).
706 https://doi.org/10.1371/JOURNAL.PPAT.1007405.

707 29. Kumar V. Natural killer cells in sepsis: Underprivileged innate immune
708 cells. *Eur J Cell Biol*. 2019;98(2–4):81–93.

709 30. Nati M, Chung K-J, Chavakis T. The Role of Innate Immune Cells in
710 Nonalcoholic Fatty Liver Disease Introduction: MAFLD and NASH. [published
711 online ahead of print: 2021]. https://doi.org/10.1159/000518407.

712 31. Li M, et al. Recent advances targeting C-C chemokine receptor type 2 for
713 liver diseases in monocyte/macrophage. *Liver Int*. 2020;40(12):2928–2936.

714 32. Metzemaekers M, Gouwy M, Proost P. Neutrophil chemoattractant
715 receptors in health and disease: double-edged swords. *Cellular & Molecular*
716 *Immunology 2020 17:5*. 2020;17(5):433–450.

717 33. Eriguchi Y, et al. Essential role of IFN-γ in T cell–associated intestinal
718 inflammation. *JCI Insight*. 2018;3(18).
719 https://doi.org/10.1172/JCI.INSIGHT.121886.

720 34. Lin Q, et al. IFN-γ-dependent NK cell activation is essential to metastasis
721 suppression by engineered Salmonella. *Nat Commun*. 2021;12(1).
722 https://doi.org/10.1038/S41467-021-22755-3.

723 35. Arase H, Arase N, Saito T. Interferon gamma production by natural killer
724 (NK) cells and NK1.1+ T cells upon NKR-P1 cross-linking. *J Exp Med*.
725 1996;183(5):2391–2396.

726 36. Wang J feng, et al. Upregulated PD-L1 delays human neutrophil apoptosis
727 and promotes lung injury in an experimental mouse model of sepsis. *Blood*.
728 2021;138(9):806–810.

729 37. Falcinelli M, et al. Propranolol reduces IFN-γ driven PD-L1
730 immunosuppression and improves anti-tumour immunity in ovarian cancer.
731 *Brain Behav Immun*. 2023;110:1–12.

732 38. Acharya C, Bajaj JS. Gut Microbiota and Complications of Liver Disease.
733 *Gastroenterol Clin North Am*. 2017;46(1):155–169.

734 39. Mohammad S, Thiemermann C. Role of Metabolic Endotoxemia in
735 Systemic Inflammation and Potential Interventions. *Front Immunol*. 2021;11.
736 https://doi.org/10.3389/FIMMU.2020.594150.

737 40. Chen Y, Tian Z. Roles of Hepatic Innate and Innate-Like Lymphocytes in
738 Nonalcoholic Steatohepatitis. *Front Immunol*. 2020;11.
739 https://doi.org/10.3389/FIMMU.2020.01500.

740 41. Hwang S, et al. Role of Neutrophils in the Pathogenesis of Nonalcoholic
741 Steatohepatitis. *Front Endocrinol (Lausanne)*. 2021;12.
742 https://doi.org/10.3389/FENDO.2021.751802.

743 42. Stiglund N, et al. Retained NK Cell Phenotype and Functionality in Non-
744 alcoholic Fatty Liver Disease. *Front Immunol*. 2019;10(JUN).
745 https://doi.org/10.3389/FIMMU.2019.01255.

746 43. Mantovani A, et al. Neutrophils in the activation and regulation of innate
747 and adaptive immunity. [published online ahead of print: 2011].
748 https://doi.org/10.1038/nri3024.

749 44. Zeerleder S, et al. Activated cytotoxic T cells and NK cells in severe sepsis
750 and septic shock and their role in multiple organ dysfunction. *Clin Immunol*.
751 2005;116(2):158–165.

752 45. Luo XY, et al. IFN-γ deficiency attenuates hepatic inflammation and fibrosis
753 in a steatohepatitis model induced by a methionine- and choline-deficient high-
754 fat diet. *Am J Physiol Gastrointest Liver Physiol*. 2013;305(12).
755 https://doi.org/10.1152/AJPGI.00193.2013.

756 46. Rosales C. Neutrophil: A Cell with Many Roles in Inflammation or Several
757 Cell Types? *Front Physiol*. 2018;9(FEB).
758 https://doi.org/10.3389/FPHYS.2018.00113.

759 47. Kanashiro A, et al. The role of neutrophils in neuro-immune modulation
760 HHS Public Access. https://doi.org/10.1016/j.phrs.2019.104580.

761 48. Tracey KJ, et al. Shock and tissue injury induced by recombinant human
762 cachectin. *Science*. 1986;234(4775):470–474.

763 49. Bordon J, et al. Understanding the roles of cytokines and neutrophil activity
764 and neutrophil apoptosis in the protective versus deleterious inflammatory
765 response in pneumonia. *Int J Infect Dis*. 2013;17(2).
766 https://doi.org/10.1016/J.IJID.2012.06.006.

50. Leslie J, et al. CXCR2 inhibition enables NASH-HCC immunotherapy. *Gut*. 2022;71(10):2093–2106.

51. Dong G, et al. Increased PD-L1 Restricts Liver Injury in Nonalcoholic Fatty Liver Disease. *Oxid Med Cell Longev*. 2022;2022. https://doi.org/10.1155/2022/5954437.

52. Thanabalasuriar A, et al. *H E A L T H A N D M E D I C I N E PD-L1 + neutrophils contribute to injury-induced infection susceptibility*. 2021.

53. Huston JM, et al. Splenectomy inactivates the cholinergic antiinflammatory pathway during lethal endotoxemia and polymicrobial sepsis. *J Exp Med*. 2006;203(7):1623–1629.

54. Fonseca MT, et al. A leukotriene-dependent spleen-liver axis drives TNF production in systemic inflammation. *Sci Signal*. 2021;14(679). https://doi.org/10.1126/SCISIGNAL.ABB0969.

55. R: a language and environment for statistical computing [Internet]. https://www.gbif.org/tool/81287/r-a-language-and-environment-for-statistical-computing. Accessed April 18, 2024.

56. Hao Y, et al. Integrated analysis of multimodal single-cell data. *Cell*. 2021;184(13):3573-3587.e29.

57. Wickham H. ggplot2. [published online ahead of print: 2016]. https://doi.org/10.1007/978-3-319-24277-4.

58. scCustomize-package: scCustomize: Custom Visualizations & Functions for... in samuel-marsh/scCustomize: Custom Visualizations & Functions for Streamlined Analyses of Single Cell Sequencing [Internet]. https://rdrr.io/github/samuel-marsh/scCustomize/man/scCustomize-package.html. Accessed April 18, 2024.

59. Chen Y, Lun ATL, Smyth GK. From reads to genes to pathways: Differential expression analysis of RNA-Seq experiments using Rsubread and the edgeR quasi-likelihood pipeline. *F1000Res*. 2016;5. https://doi.org/10.12688/F1000RESEARCH.8987.2/DOI.

60. Wu T, et al. clusterProfiler 4.0: A universal enrichment tool for interpreting omics data. *Innovation (Cambridge (Mass))*. 2021;2(3). https://doi.org/10.1016/J.XINN.2021.100141.

805

806 **Figure 1. Mice fed with a high-fat and choline-deficient (HFCD) diet develop**
807 **Metabolically Dysfunctional-Associated Fatty Liver Disease (MAFLD) and are more**
808 **susceptible to endotoxemia.** (A) Schematic illustration of the experimental design. (B)
809 Survival curves of mice with MAFLD (n=5) and Chow diet (controls) (n=5) which were
810 injected intraperitoneally with LPS (10mg/kg) and the survival rates were determined
811 daily for 7 days (C and D) Serum ALT and Urea levels from mice with MAFLD and
812 Chow, 6 hours after LPS (10 mg/kg) and PBS administration (n=5). (E) Effect of LPS
813 inoculation on histopathology (H&E stain) of liver from mice with MAFLD or controls
814 (Chow diet). The results are expressed as the mean ± standard deviation (SD) from
815 one representative experiment. Statistical analysis was performed using one-way
816 ANOVA followed by Tukey's multiple comparison test. Statistical significance was
817 determined with the following p-values: *$p < 0.05$, **$p < 0.01$, ***$p < 0.001$. Each
818 experiment was independently repeated 2 times to ensure reproducibility of the
819 findings.

820

821

822 **Figure 2. The expression of genes from the inflammatory pathways of IFN-γ and**
823 **TNF-α is increased during the development of MAFLD in mice and humans.** (A)
824 Volcano plots illustrating the fold change and P-value for gene expression
825 comparisons between livers of MAFLD and healthy patients. Genes of interest are
826 highlighted on the volcano charts. (B) Gene Ontology (GO) functional analysis of
827 differentially expressed genes (DEGs). GO enrichment analysis of DEGs was
828 conducted using DAVID, presenting the 20 most significantly ($P < 0.05$) enriched GO
829 terms in biological process, molecular function, and cellular component categories. All
830 adjusted statistically significant values are presented as negative log-transformed
831 base 10 values. (C) UMAP plots depicting immune cells from the livers of mice
832 subjected to 30 weeks of HFCD diet compared to Chow diet. (D) Frequency
833 distribution of immune cell populations. (E) Expression levels of CD14, CD274, IFN-γ,
834 and TNF-α genes within hepatic immune cell populations.

835

836 **Figure 3. TNF-α and IFN-γ participate in susceptibility in mice with MAFLD to**
837 **endotoxemia.** (A) IFN-γ and (B) TNF-α secretion in the tissue livers of Chow and
838 MAFLD mice injected with LPS (10mg/kg) (n = 5). (C) Serum ALT levels from mice
839 with MAFLD and Chow and/or knockout of IFNγ (IFNγ-/-) and (D) TNFα (TNFR1R2-/-
840), 6 hours after 10 mg/kg LPS and PBS administration (n=5). (E) Effect of LPS
841 inoculation on liver histopathology from mice with MAFLD and Chow and/or knockout
842 of IFNγ-/- and TNF-α (TNFR1R2-/-). (F) Survival curves of mice with MAFLD (n=5)
843 and Chow (n=5) and/or knockout of IFN-γ (IFN-γ-/-) and (G) TNF-α (TNFR1R2-/-),
844 after intraperitoneal inoculation of LPS (10mg/kg). The results are expressed as the
845 mean ± standard deviation (SD) from one representative experiment. Statistical
846 analysis was performed using one-way ANOVA followed by Tukey's multiple
847 comparison test. Statistical significance was determined with the following p-values:
848 *p < 0.05, **p < 0.01, ***p < 0.001. Each experiment was independently repeated 2
849 times to ensure reproducibility of the findings.

850

851 **Figure 4. IFN-γ secreted by NK cells increases susceptibility of animals with**
852 **MAFLD to endotoxemia**. (A) CD4 IFN-γ^+ and (B) CD8 IFN-γ^+ T cell frequency in
853 animals with MAFLD and Chow 6h after LPS inoculation. (C) displays survival curves
854 of mice with MAFLD (n=5) and Chow (n=5) and T-cell knockout (RAg-/-). (D) Serum
855 ALT levels from mice with MAFLD in knockout of Rag -/-, 6 hours after 10 mg/kg LPS
856 (n=5). (E) and (F) represent the number of cells and frequency of NK IFNγ^+ or IFN-γ^-
857 in animals with MAFLD and Chow 6h after LPS inoculation (G) The survival curves of
858 mice with MAFLD (n=5) and Chow (n=5) and/or depleted NK cells (Anti NK 1.1), 6
859 days after intraperitoneal inoculation of LPS (10mg/kg) (H) presents the serum ALT
860 levels from mice with MAFLD and Chow of mice with MAFLD (n=5) and Chow (n=5)
861 and/or depleted NK cells (Anti NK 1.1), 6 hours after 10 mg/kg LPS or PBS
862 administration (n=5). (I) and (J) depict IFN-γ and TNF-α secretion in the livers of Chow
863 and MAFLD mice injected with LPS (10mg/kg) (n=5), respectively. (K) shows TNF-α
864 secretion in the livers of Chow and MAFLD and/or knockout of IFN-γ (IFNγ-/-) mice
865 injected with LPS (10mg/kg) (n=5)." The results are expressed as the mean ± standard
866 deviation (SD) from one representative experiment. Statistical analysis was performed
867 using one-way ANOVA followed by Tukey's multiple comparison test. Statistical
868 significance was determined with the following p-values: *p < 0.05, **p < 0.01, ***p <
869 0.001. Each experiment was independently repeated 2 times to ensure reproducibility
870 of the findings.

871

872

873

874

875

876 **Figure 5. Neutrophils but not monocytes mediate susceptibility of animals with**
877 **MAFLD to endotoxemia** (A) Representative flow cytometry plot showing monocytes
878 (CD45+CD11b+MHC-Ly6C+Ly6G-) and neutrophils (CD45+CD11b+MHC-
879 Ly6C+Ly6G+) and a number of monocytes (B) and neutrophils (C) in animals with
880 MAFLD and Chow after LPS inoculation. (D) Effect of LPS inoculation on liver
881 histopathology of mice with MAFLD and Chow treated with a CXCR2 inhibitor
882 (CXCR2i) and neutrophil-depleted animals (anti-Ly6G). (E) Serum ALT levels of mice
883 with MAFLD and Chow and/or CXCR2i and anti-Ly6G, 6 hours after administration of
884 10 mg/kg of LPS and PBS (n=5). (F) TNF-α secretion in the liver of Chow and MAFLD
885 mice injected with LPS (10mg/kg) (n = 5). (G) Survival curves of mice with MAFLD
886 (n=5) and Chow (n=5) treated with anti-Ly6G or (H) CXCR2i, and the survival rates
887 were analysed daily for 6 days after intraperitoneal administration of LPS (10mg/kg).
888 The results are expressed as the mean ± standard deviation (SD) from one
889 representative experiment. Statistical analysis was performed using one-way ANOVA
890 followed by Tukey's multiple comparison test. Statistical significance was determined
891 with the following p-values: *p < 0.05, **p < 0.01, ***p < 0.001. Each experiment was
892 independently repeated 2 times to ensure reproducibility of the findings.

893

894 **Figure 6. IFN-γ induces PD-L1 expression and reduces apoptosis in mouse**
895 **neutrophils with MAFLD.** (A) Representative flow cytometry plot showing the
896 expression of PD-L1 in gated neutrophils and (B) the quantification of PD-L1+
897 neutrophils in the liver of mice with MAFLD or that received Chow diet, 6 hours after
898 LPS inoculation (n=5 per group). (C) Representative flow cytometry plot showing the
899 expression of PD-L1 in gated neutrophils and (D) the quantification of PD-L1+
900 neutrophils in the liver of mice with MAFLD and Chow and/or IFNγ knockout (IFNγ-/-)
901 6 hours after LPS inoculation (n=5 per group). (E) Representative flow cytometry plot
902 showing the expression of PD-L1 and apoptosis (Annexin V+ 7AAD+) in gated
903 neutrophils and (F) the frequency of apoptosis in neutrophils cultured in medium, LPS,
904 IFN-γ, or LPS+ IFN-γ for 24 hours. The results are expressed as the mean ± standard
905 deviation (SD) from one representative experiment. Statistical analysis was performed
906 using one-way ANOVA followed by Tukey's multiple comparison test. Statistical
907 significance was determined with the following p-values: *p < 0.05, **p < 0.01, ***p <
908 0.001. Each experiment was independently repeated 2 times to ensure reproducibility
909 of the findings.

910

Figure 7. IFN-γ-dependent secretion of TNF-α by PD-L1+ neutrophils induces susceptibility of animals with MAFLD to endotoxemia. (A) Representative flow cytometry plot showing TNF-α expression in PD-L1+ neutrophils in the liver of animals with MAFLD or fed with Chow diet 6h after LPS inoculation. (B) Number of TNF-α+ neutrophils. (C) Number of TNF-α+PD-L1- neutrophils. (D) number of TNF-α+PD-L1+ neutrophils. (E) Representative flow cytometry plot showing TNF-α expression in PD-L1+TNF+ neutrophils in the liver of animals with MAFLD and Chow and/or depleted NK cells (anti-NK 1.1) 6h after LPS inoculation. (F) Number of PD-L1+ neutrophils. (G) Frequency of TNF-α+ neutrophils. The results are expressed as the mean ± standard deviation (SD) from one representative experiment. Statistical analysis was performed using one-way ANOVA followed by Tukey's multiple comparison test. Statistical significance was determined with the following p-values: *$p < 0.05$, **$p < 0.01$, ***$p < 0.001$. Each experiment was independently repeated 2 times to ensure reproducibility of the findings.

Figure 8. Anti PD-L1 treatment reduces PD-L1 neutrophils in animals with MAFLD during endotoxemia. (A) Schematic illustration of experimental design. (B) Serum ALT levels of mice with MAFLD or feded with Chow and/or treated with anti-PDL1, 6 hours after administration of 10 mg/kg of LPS or PBS (n=5). (C) IFN-γ and TNF-α secretion in the liver of Chow and MAFLD mice injected with LPS (10mg/kg) treated with anti-PDL1 (n = 5). (D) Survival curves of mice with MAFLD (n=5) and Chow (n=5) treated or not with anti-PD-L1. (E) Representative flow cytometry graph showing TNF-α expression in PD-L1+ neutrophils in the liver of animals with MAFLD and Chow and/or treated with anti-PD-L1 6h after LPS inoculation. (F) Effect of LPS inoculation in liver histopathology of mice with MAFLD and Chow treated or not with anti-PD-L1. (G and J) Frequency of PDL1 neutrophils, (H and K) Number of neutrophils, (I and L) Number of NK cells from animals with MAFLD and Chow and/or treated with anti-PDL1 after 6h of LPS inoculation. The results are expressed as the mean ± standard deviation (SD) from one representative experiment. Statistical analysis was performed using one-way ANOVA followed by Tukey's multiple comparison test. Statistical significance was determined with the following p-values: *$p < 0.05$, **$p < 0.01$, ***$p < 0.001$. Each experiment was independently repeated 2 times to ensure reproducibility of the findings.

Figure S1. Validation of the HFCD-induced MAFLD experimental model based on liver weight, blood glucose levels, and histological analysis (H&E and Picro Sirius staining). (A) Liver height, (B) plasma glucose, and (C) representative liver histological sections of lipid accumulation, steatotic morphology and collagen deposition (Picro Sirius Red staining) of mice fed a high-fat, choline-deficient (HFCD) or control chow diet for two weeks and subsequently challenged or not with LPS (10 mg/kg, i.p.)(n=5) (Data are expressed as the mean ± standard deviation (SD) from one representative experiment. Statistical analysis was performed using one-way ANOVA followed by Tukey's multiple

954 comparison test. Statistical significance was determined as *p < 0.05, **p < 0.01, ***p
955 < 0.001. Each experiment was independently repeated at least twice to ensure
956 reproducibility of the findings

957 **Figure S2. The IFNγ-deficient mice display LPS responses comparable to**
958 **controls.**
959 (A–B) Splenocytes isolated from C57BL/6 and IFNγ^{-}/$^{-}$ mice fed with Chow or HFCD
960 for two weeks were stimulated in vitro with LPS (100 ng/mL) for 24 hours. Cytokine
961 levels of (A) IL-6 and (B) TNF-α were quantified in the culture supernatants. Data are
962 expressed as mean ± standard deviation (SD) from one representative experiment (n
963 = 5 per group). Statistical analysis was performed using one-way ANOVA followed by
964 Tukey's multiple comparison test. Statistical significance was defined as *p < 0.05, **p
965 < 0.01, ***p < 0.001. Each experiment was independently repeated twice to ensure
966 reproducibility.

967 **Figure S3. NK cells produce high levels of IFN-γ during endotoxemia in MAFLD**
968 (A) Representative flow cytometry dot plot showing CD4^{+}IFN-γ^{+} T cells from the liver
969 of mice fed a high-fat, choline-deficient (HFCD) or chow diet for two weeks and
970 subsequently challenged or not with LPS. (B) Representative dot plot of hepatic
971 CD8^{+}IFN-γ^{+} T cells under the same experimental conditions. (C) Representative dot
972 plot showing NK cells (NK1.1^{+}CD3^{-}) from the liver of HFCD and chow-fed mice
973 challenged or not with LPS. (D) Representative dot plot of IFN-γ expression by NK
974 cells (NK1.1^{+}CD3^{-}) from the same groups.

975 **Figure S4. Anti-NK1.1 treatment depletes NK cells in animals with MAFLD during**
976 **endotoxemia**
977 (A) Representative flow cytometry dot plot showing depletion of NK cells
978 (NK1.1^{+}CD3^{-}) in the liver of mice fed a high-fat, choline-deficient (HFCD) or chow diet
979 for two weeks and challenged with LPS, following treatment with anti-NK1.1 antibody.

980 **Figure S5. Monocytes do not participate in the susceptibility of mice with**
981 **MAFLD to endotoxemia**
982 (A) Representative flow cytometry dot plot showing neutrophils (CD45^{+}CD11b^{+}Ly6G^{+})
983 and monocytes (CD45^{+}CD11b^{+}Ly6G^{-}) in the liver of C57BL/6 and CCR2^{-}/$^{-}$ mice fed
984 a high-fat, choline-deficient (HFCD) or chow diet for two weeks and challenged with
985 LPS. (B) Survival curves of C57BL/6 and CCR2^{-}/$^{-}$ mice under the same experimental
986 conditions. (C) Representative dot plot of total leukocytes (CD45^{+}) in the liver of
987 C57BL/6 and CCR2^{-}/$^{-}$ mice after LPS challenge. (D) Frequency of leukocytes (CD45^{+})
988 in the liver of C57BL/6 and CCR2^{-}/$^{-}$ mice fed HFCD or chow diet and challenged with
989 LPS (n=5). Data are representative of one experiment reproduced independently twice
990 with similar results. Statistical analysis was performed using one-way ANOVA followed
991 by Tukey's multiple comparison test. Statistical significance was determined with the
992 following p-values: *p < 0.05, **p < 0.01, ***p < 0.001. Results are expressed as the
993 mean ± standard deviation (SD).

994 **Figure S6. Neutrophils are the main PD-L1–expressing subset among**
995 **CD45^{+}CD11b^{+} leukocytes in MAFLD.**(A and B) Representative flow cytometry
996 histogram showing PD-L1 expression on neutrophils (CD45^{+}CD11b^{+}Ly6C^{+}Ly6G^{+}) and

monocytes ($CD45^+CD11b^+Ly6C^+Ly6G^-$) isolated from the liver of mice fed a high-fat, choline-deficient (HFCD) or control chow diet for two weeks and challenged with LPS (10 mg/kg, i.p.) (n=5) (C) Representative dot plot showing PD-L1 expression within total hepatic $CD45^+CD11b^+$ leukocytes from chow- and HFCD-fed animals for two weeks, either challenged or not with LPS. (D) Representative dot plot depicting the relative proportions of neutrophils($CD45^+CD11b^+Ly6C^+Ly6G^+$) and monocytes ($CD45^+CD11b^+Ly6C^+Ly6G^-$) within total $CD45^+CD11b^+$ leukocytes in the liver of chow- and HFCD-fed mice after LPS challenge (n=5). Data are expressed as the mean ± standard deviation (SD) from one representative experiment. Statistical analysis was performed using one-way ANOVA followed by Tukey's multiple comparison test. Statistical significance was determined as *$p < 0.05$, **$p < 0.01$, ***$p < 0.001$. Each experiment was independently repeated at least twice to ensure reproducibility of the findings.

Figure S7. CXCR2i treatment reduces IFN-γ in the liver tissue of animals with MAFLD during endotoxemia
(A) IFN-γ levels in the liver of mice fed a high-fat, choline-deficient (HFCD) or chow diet for two weeks, challenged with LPS, and treated with either anti-Ly6G antibody or a CXCR2 inhibitor (CXCR2i) (n=5).. (B) IL-10 levels in the liver of the same experimental groups (n=5). The data are representative of one experiment reproduced independently twice with similar results. Statistical analysis was performed using one-way ANOVA followed by Tukey's multiple comparison test. Statistical significance was determined with the following p-values: *$p < 0.05$, **$p < 0.01$, ***$p < 0.001$. Results are expressed as the mean ± standard deviation (SD).

Figure S8. TNFR1/R2$^{-/-}$ animals do not show reduced neutrophil infiltration in the hepatic tissue of mice with MAFLD during endotoxemia. (A) Representative flow cytometry dot plot showing neutrophils ($CD45^+CD11b^+Ly6G^+$) in the liver of TNFR1R2$^{+/+}$ and TNFR1R2$^{-/-}$ mice fed a high-fat, choline-deficient (HFCD) or chow diet for two weeks and challenged with LPS. (B) Representative dot plot of PD-L1$^+$ neutrophils ($CD45^+CD11b^+Ly6G^+PD\text{-}L1^+$) under the same experimental conditions. (C) Quantification of neutrophils ($CD45^+CD11b^+Ly6G^+$) in the liver of TNFR1R2$^{+/+}$ and TNFR1R2$^{-/-}$ mice after LPS challenge. (D) Quantification of PD-L1$^+$ neutrophils ($CD45^+CD11b^+Ly6G^+PD\text{-}L1^+$) in the liver(n=5). (E) IL-10 levels in the liver of TNFR1R2$^{+/+}$ and TNFR1R2$^{-/-}$ mice fed HFCD or chow and challenged with LPS(n=5). (F) IFN-γ levels in the liver of TNFR1R2$^{+/+}$ and TNFR1R2$^{-/-}$ mice under the same conditions. (G) Representative histogram showing TNF-α expression in the liver of C57BL/6 mice fed HFCD or chow for two weeks, challenged or not with LPS. The data are representative of one experiment reproduced independently twice with similar results. Statistical analysis was performed using one-way ANOVA followed by Tukey's multiple comparison test. Statistical significance was determined with the following p-values: *$p < 0.05$, **$p < 0.01$, ***$p < 0.001$. Results are expressed as the mean ± standard deviation (SD).

1040

Figure 1. Mice fed with a high-fat and choline-deficient (HFCD) diet develop Metabolically Dysfunctional-Associated Fatty Liver Disease (MAFLD) and are more susceptible to endotoxemia

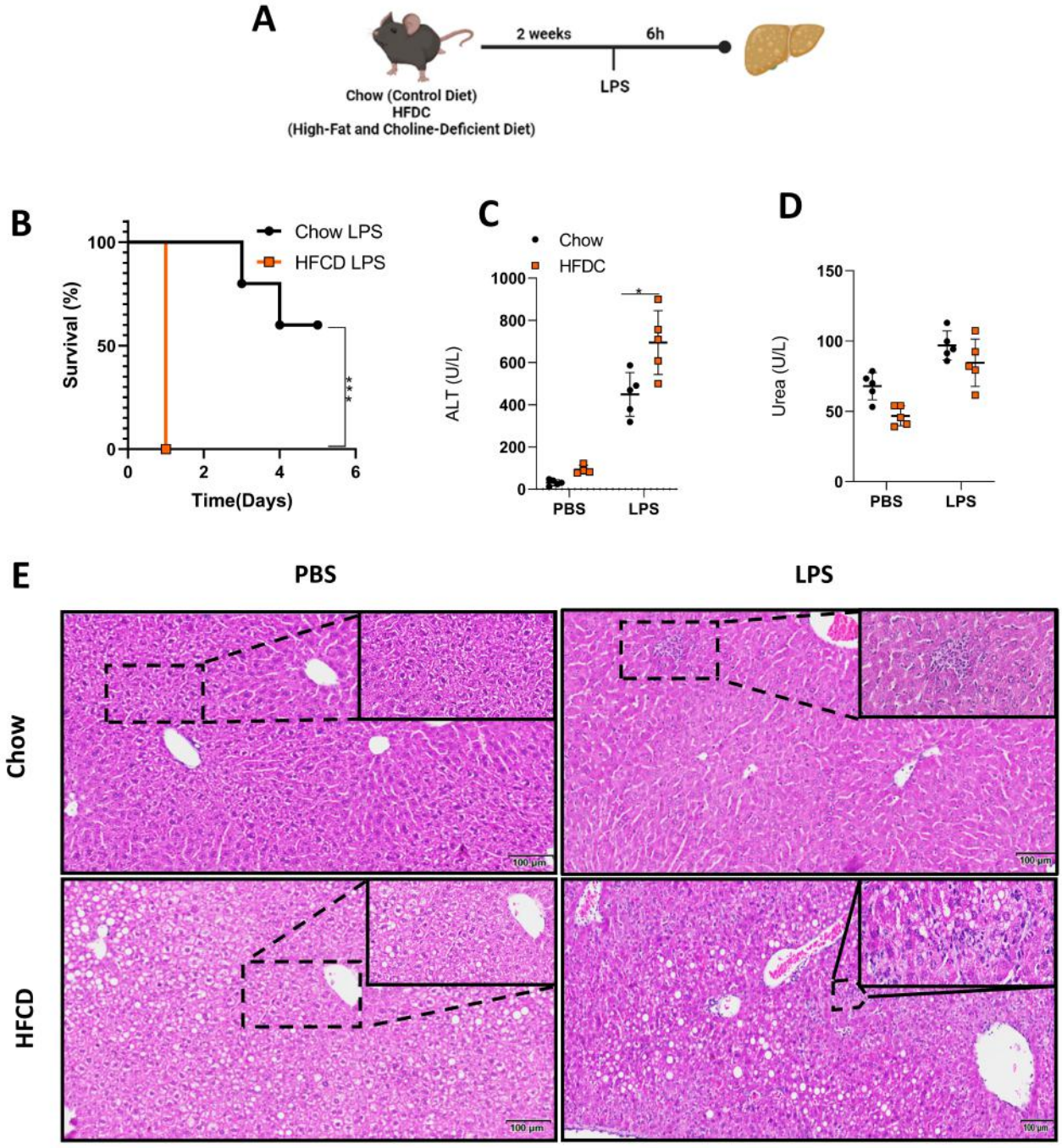

Figure 2. The expression of genes from the inflammatory pathways IFNγ and TNFα is increased during the development of MAFLD in mice and human

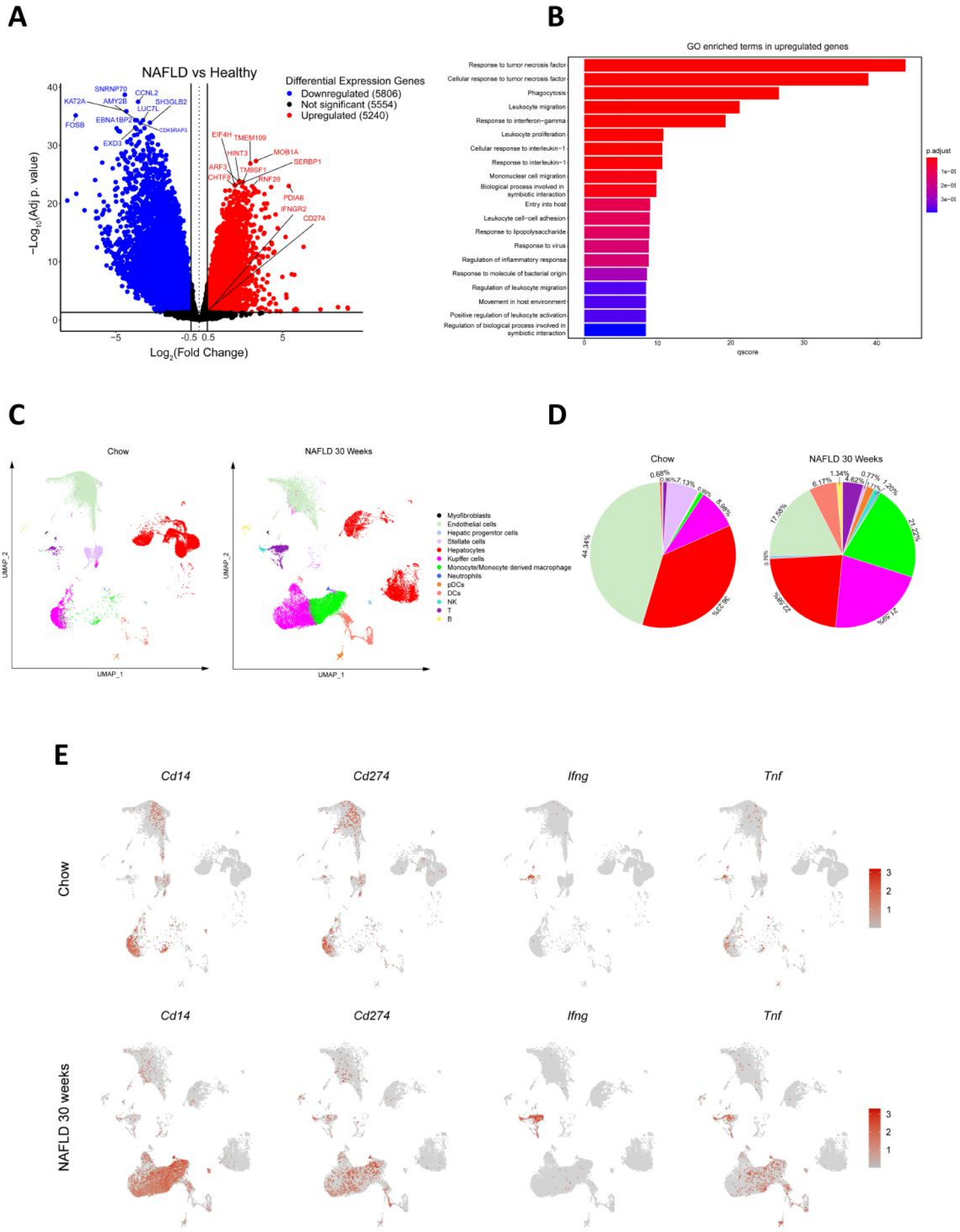

Figure 3. TNF-α and IFN-γ participate in susceptibility in mice with MAFLD to endotoxemia

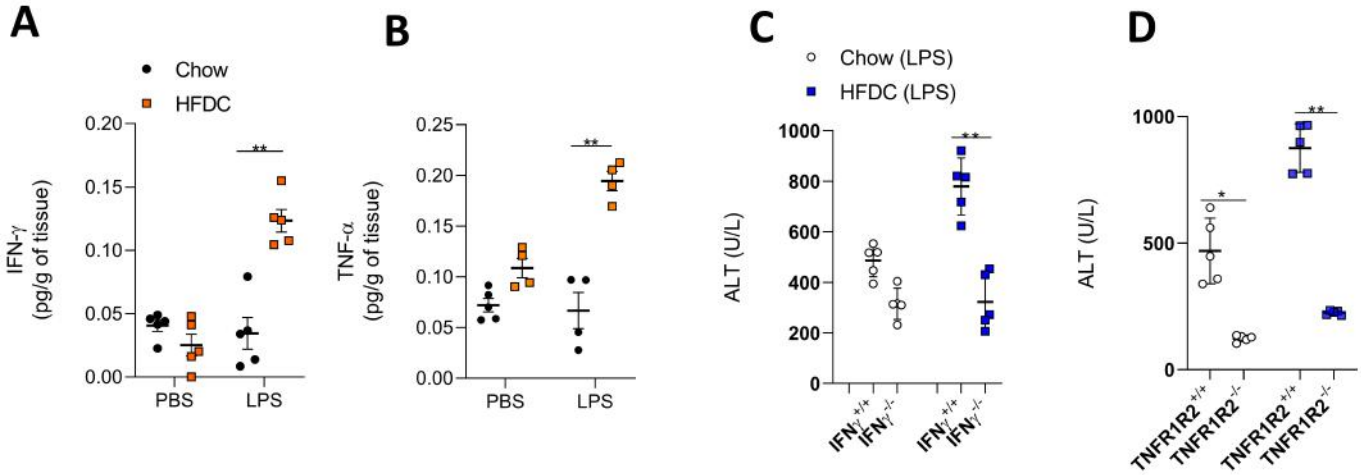

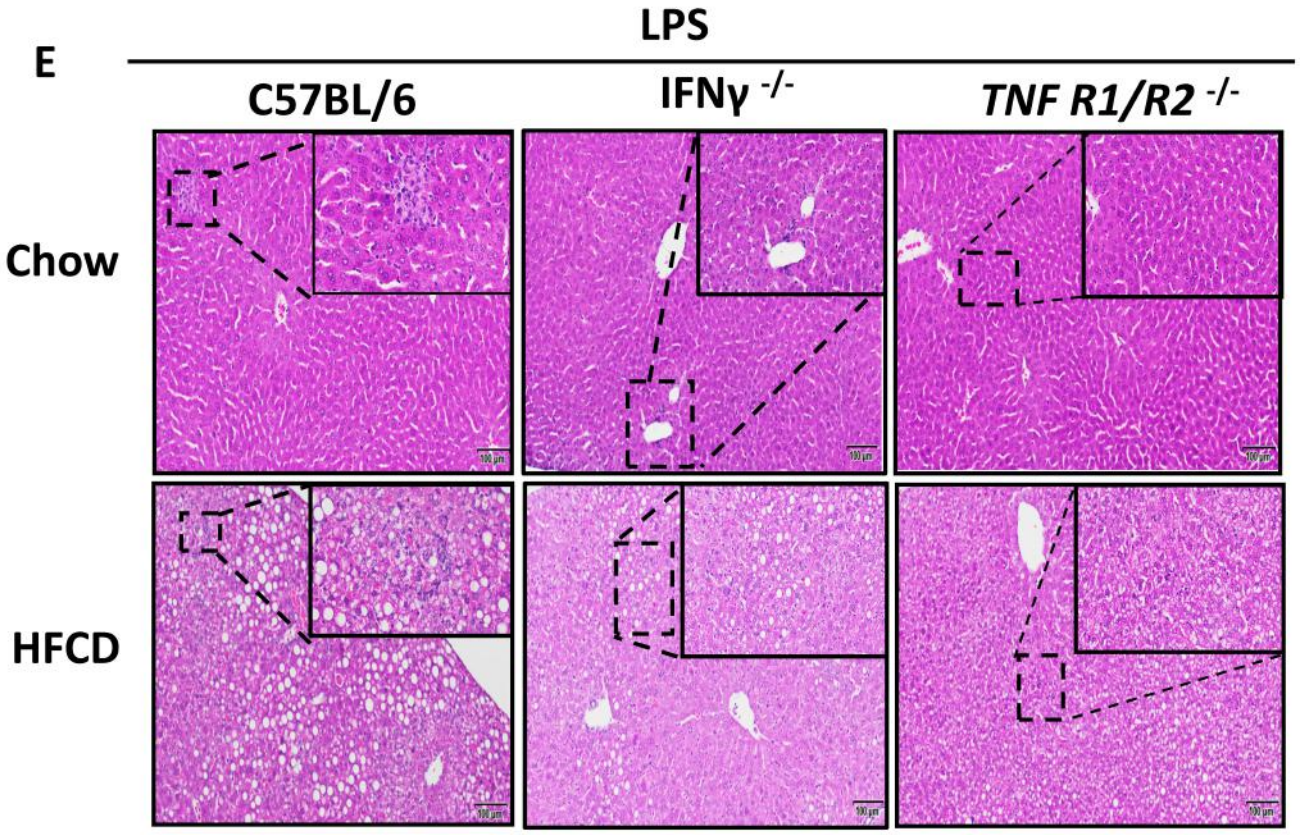

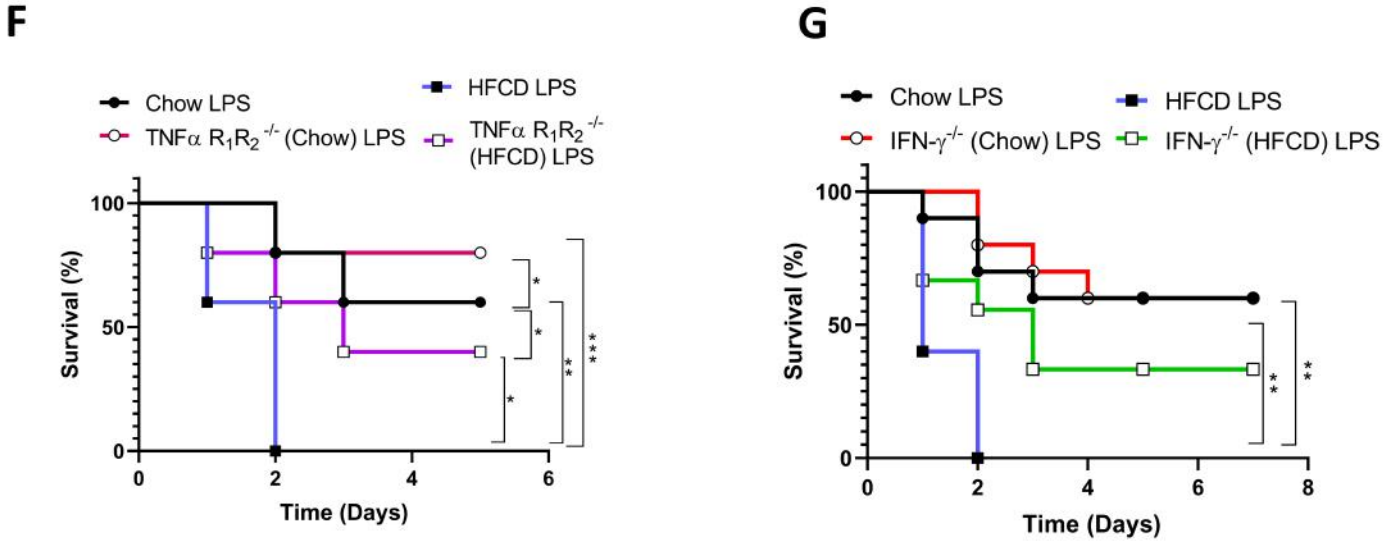

Figure 4. IFN-γ secreted by NK cells increases susceptibility of animals with MAFLD to endotoxemia

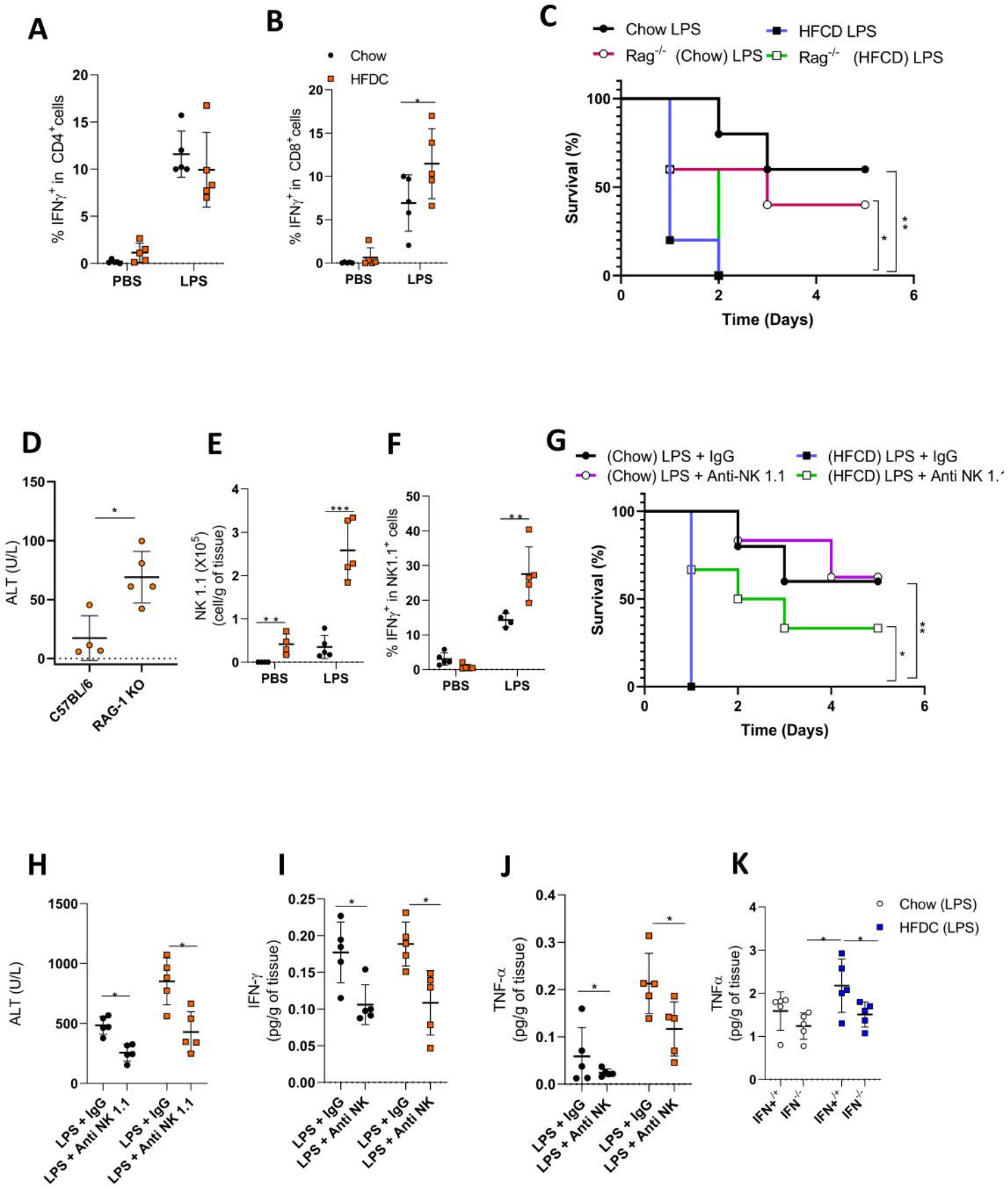

Figure 5. Neutrophils but not monocytes mediate susceptibility of animals with MAFLD to endotoxemia

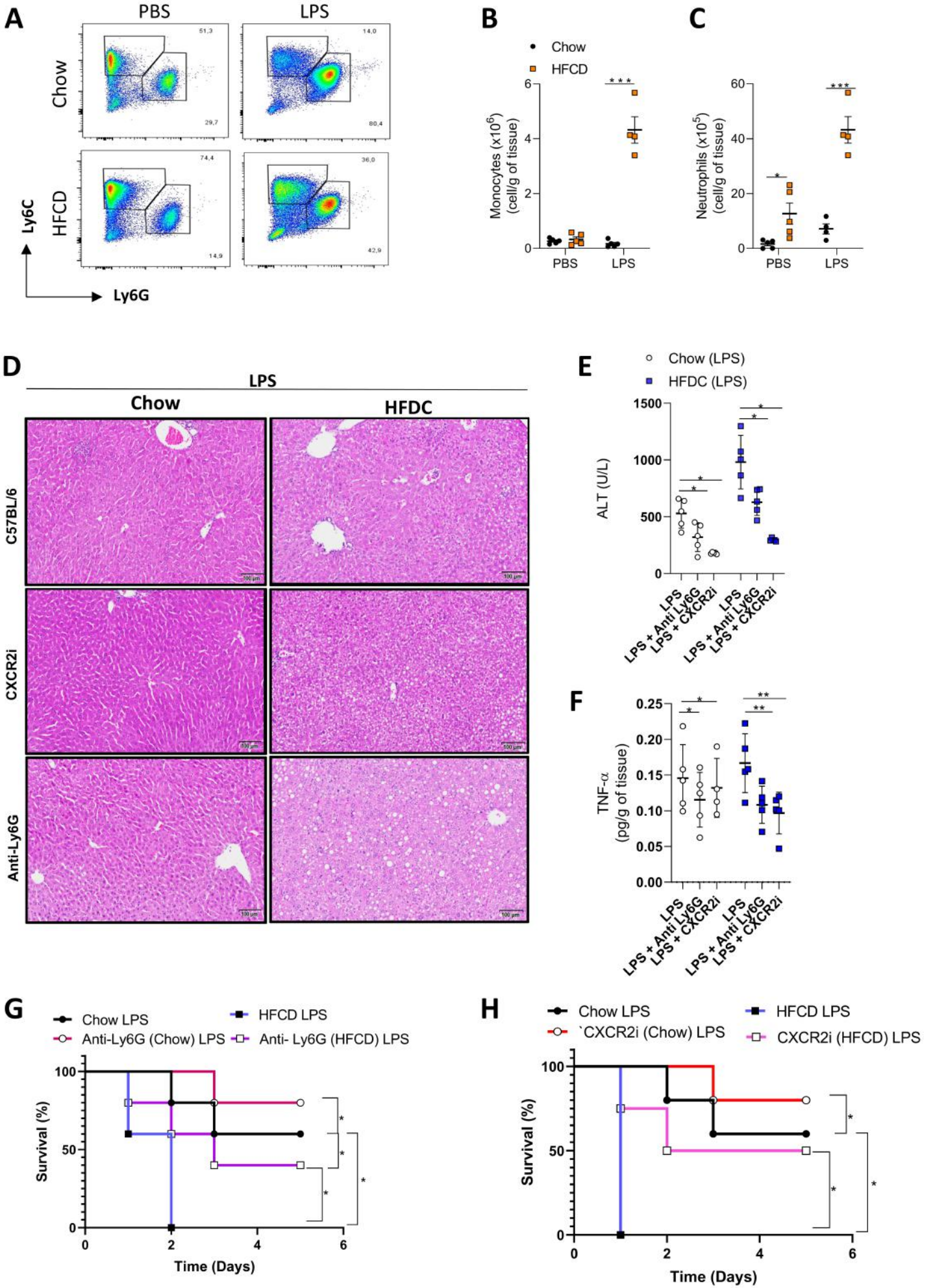

Figure 6. IFN-γ induces PD-L1 expression and reduces apoptosis in mouse neutrophils with MAFLD

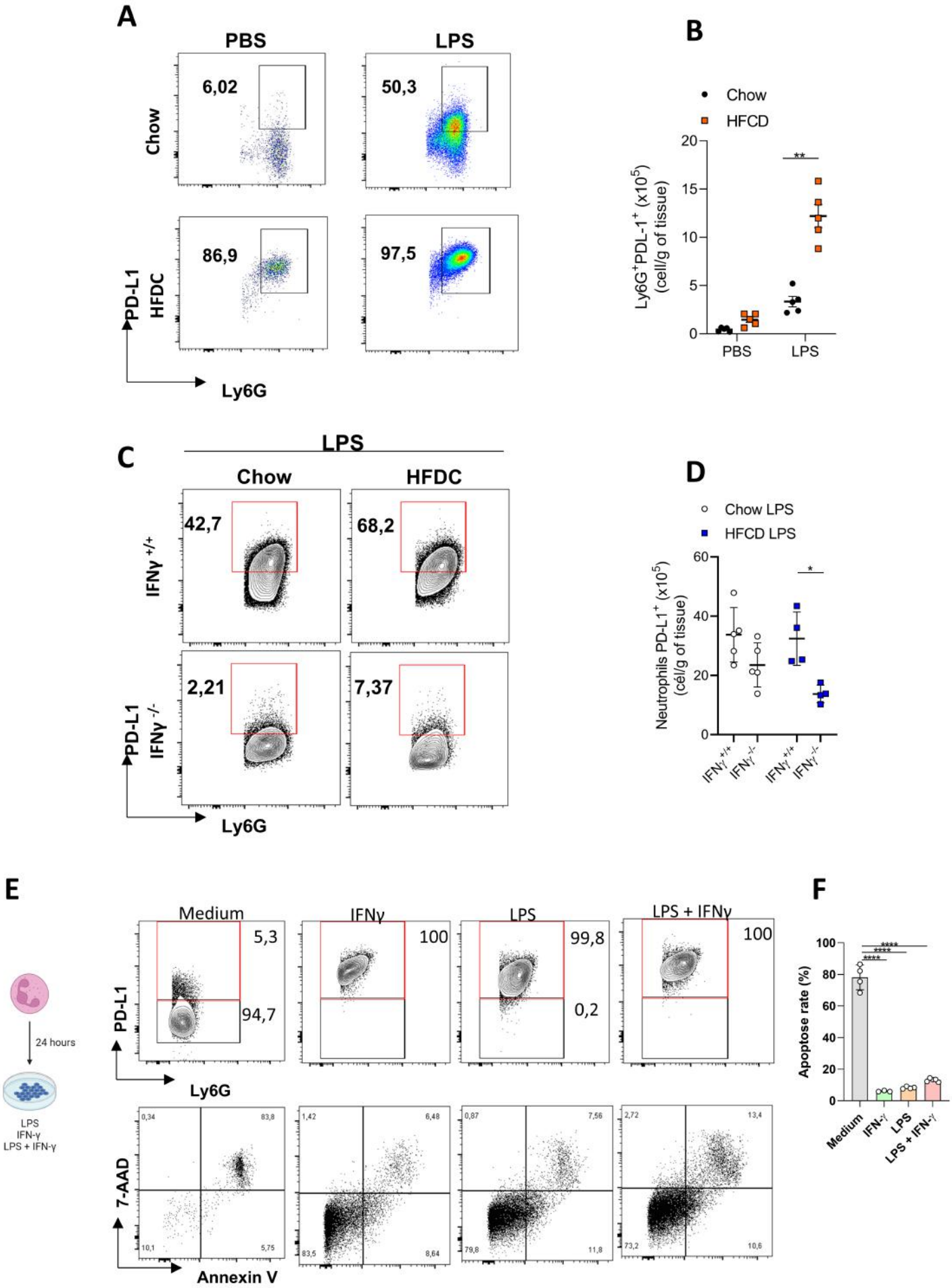

Figure 7. IFN-γ-dependent secretion of TNF-α by PD-L1+ neutrophils induces susceptibility of animals with MAFLD to endotoxemia

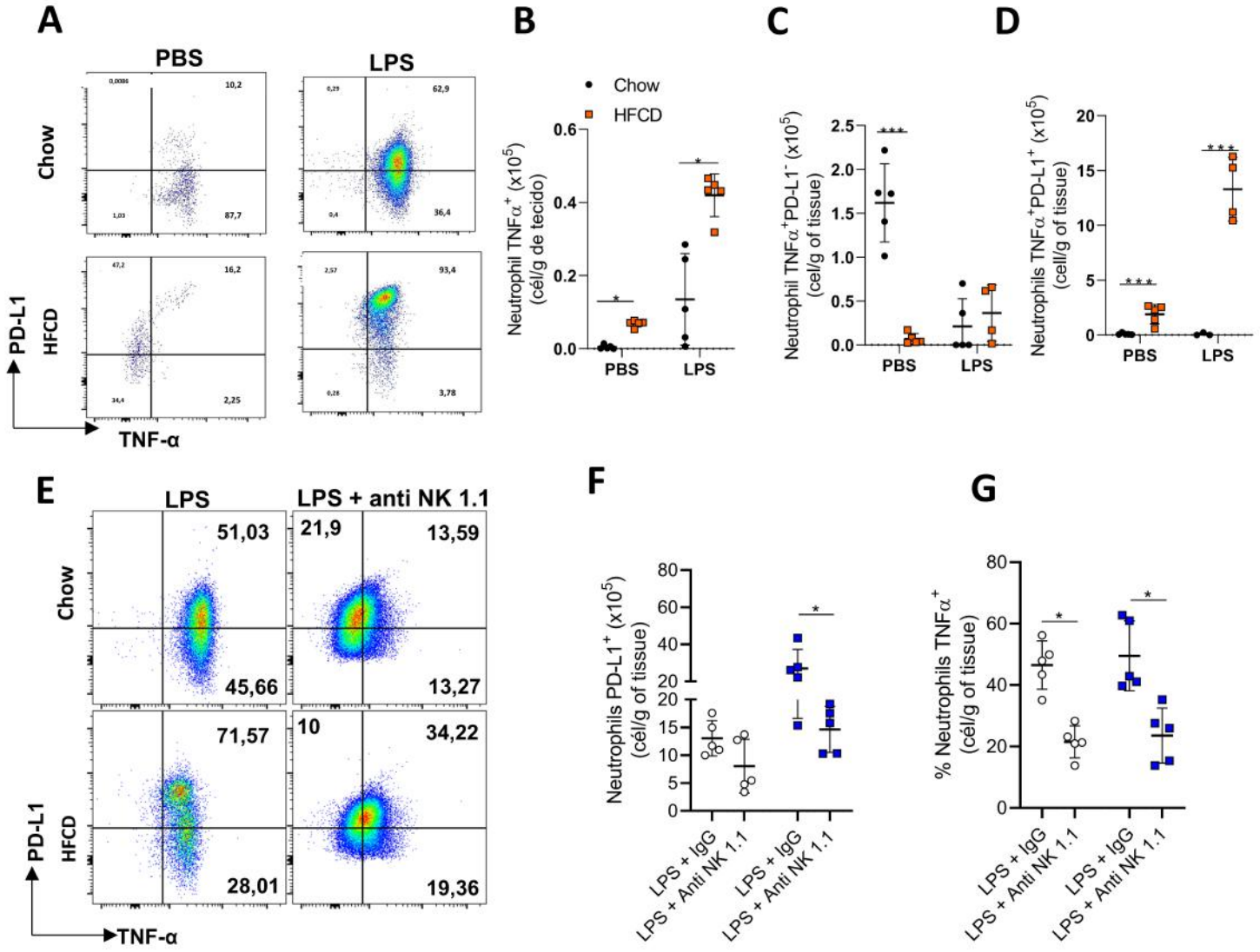

Figure 8. Anti PD-L1 treatment reduces PD-L1 neutrophils in animals with MAFLD during endotoxemia

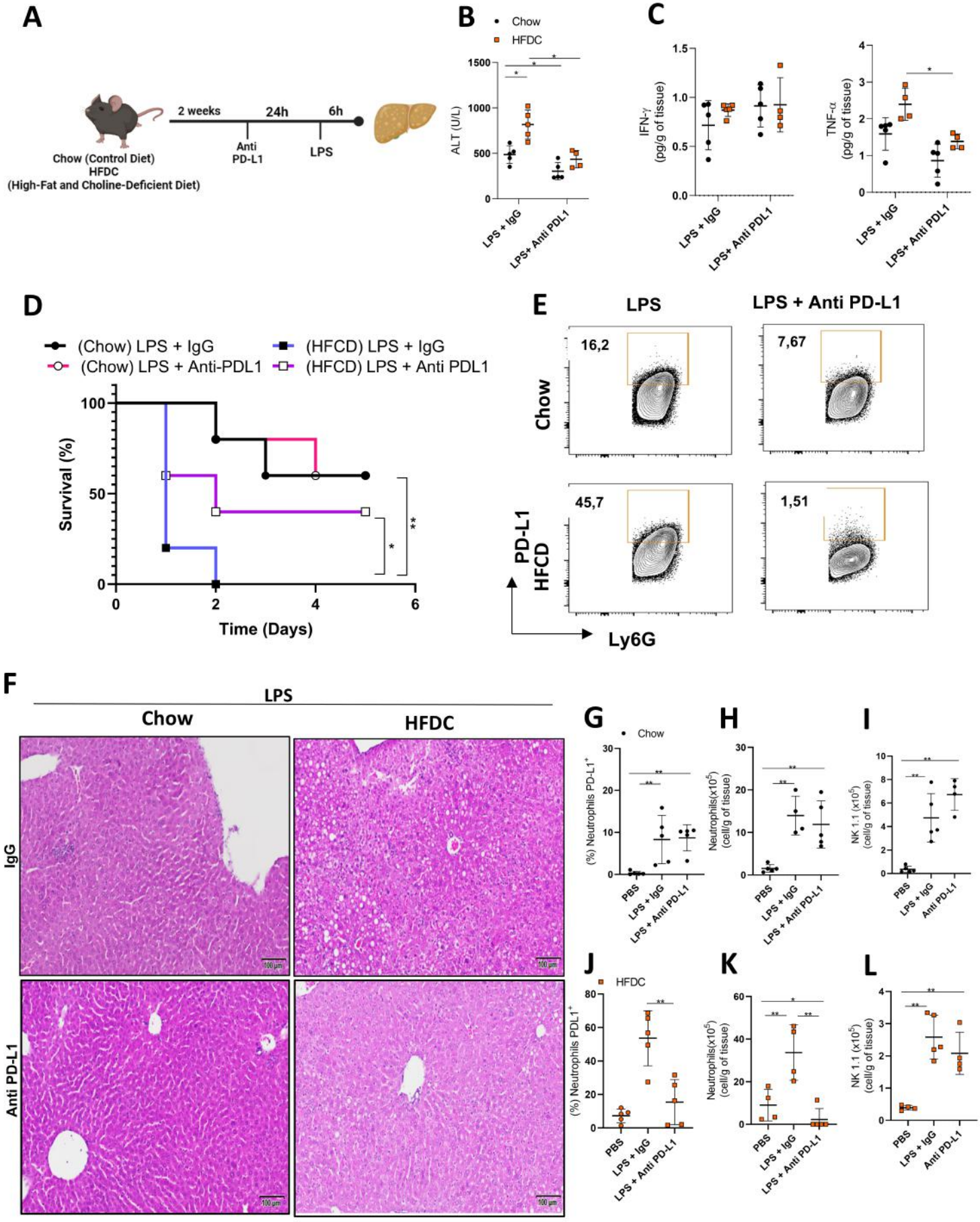

Figure S1. Validation of the HFCD-induced MAFLD experimental model based on liver weight, blood glucose levels, and histological analysis (H&E and Picro Sirius staining).

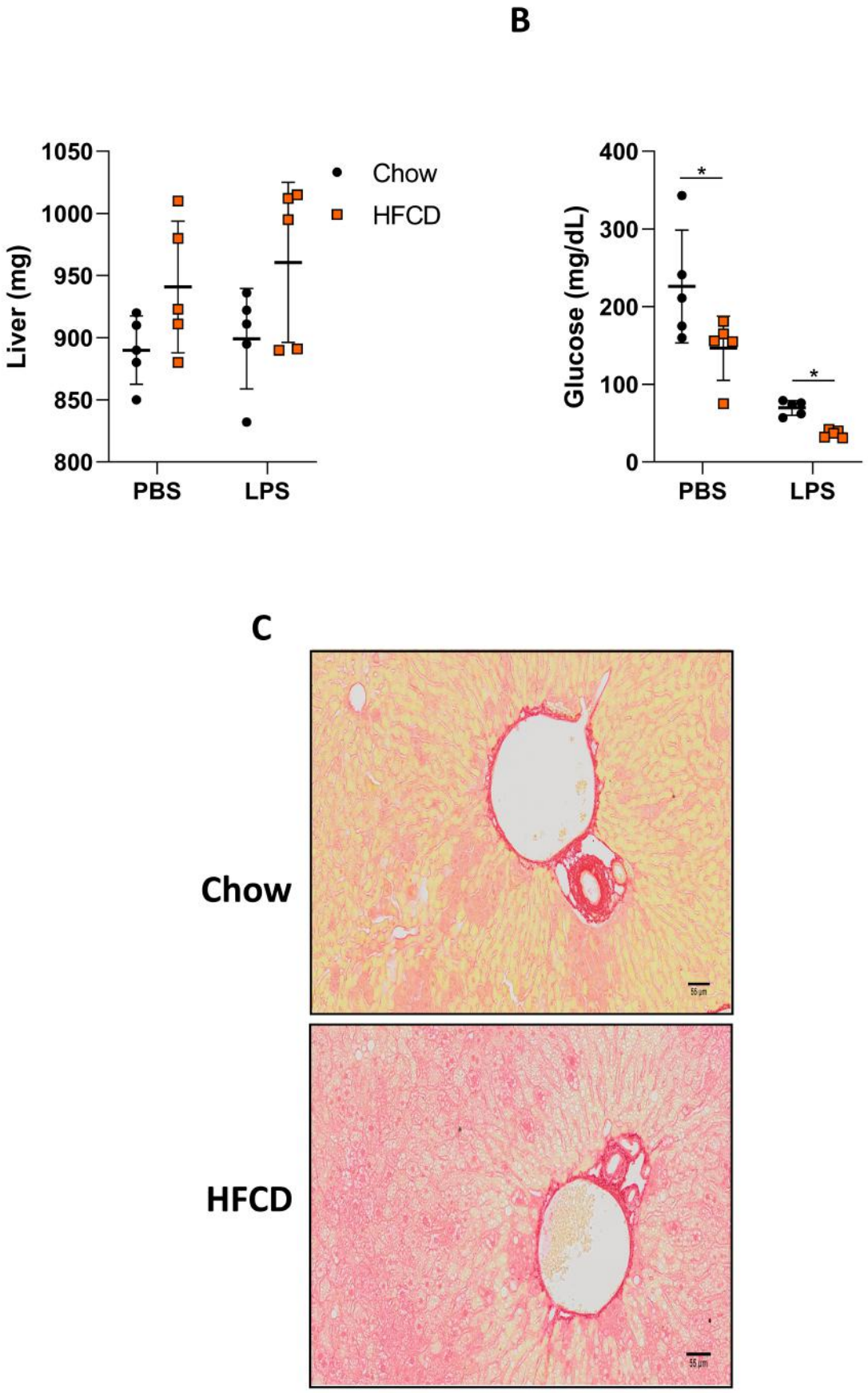

Figure S2. The IFNy-deficient mice display LPS responses comparable to controls.

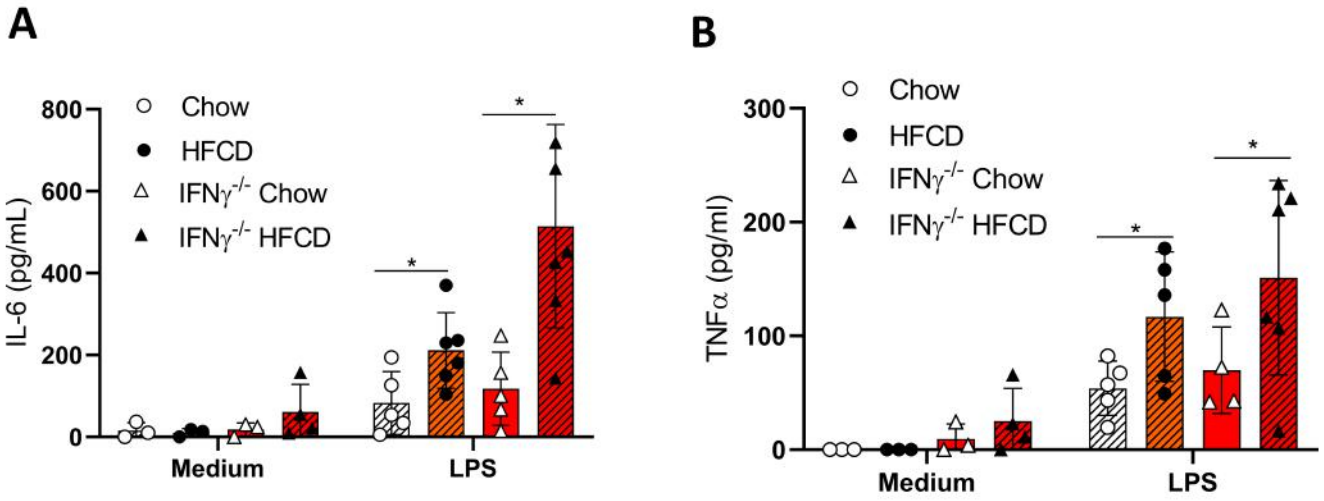

Figure S3. Nk cells produce high levels of IFN during endotoxemia in MAFLD

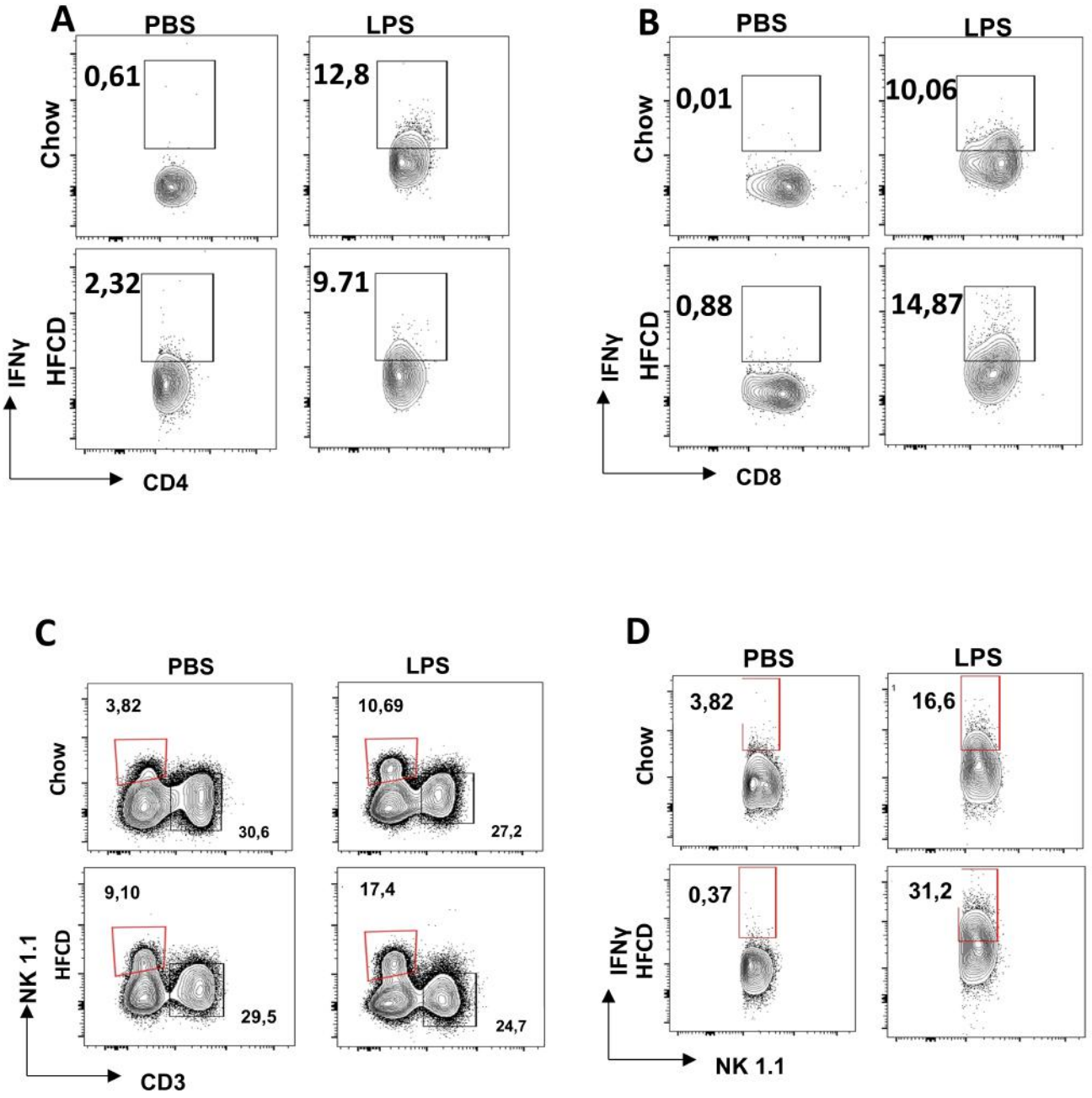

Figure S4. Anti-NK 1.1 treatment deplete NK cells in animals with MAFLD during endotoxemia

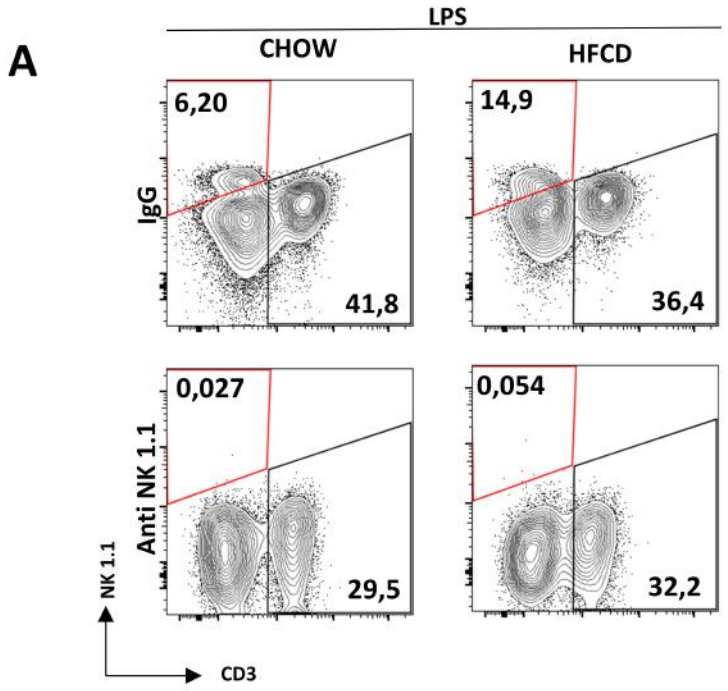

Figure S5. Monocytes do not participate in susceptibility in mice with MAFLD to endotoxemia

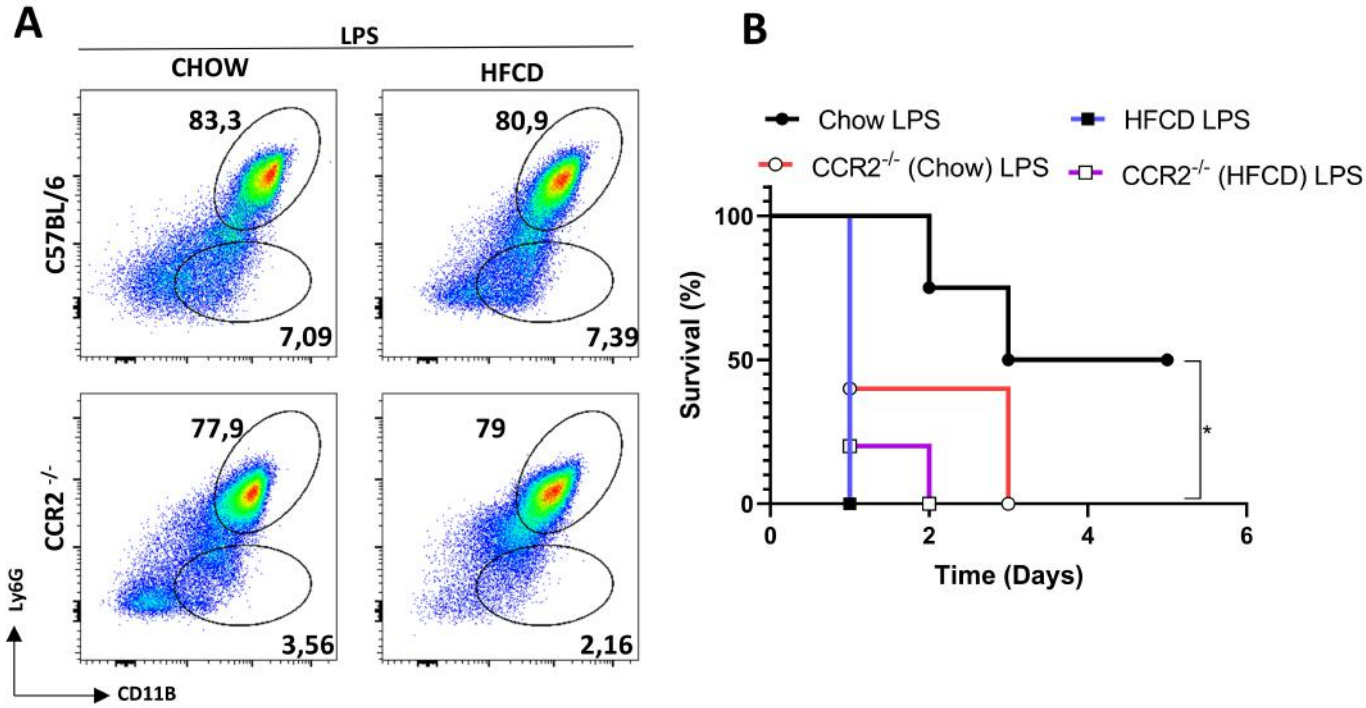

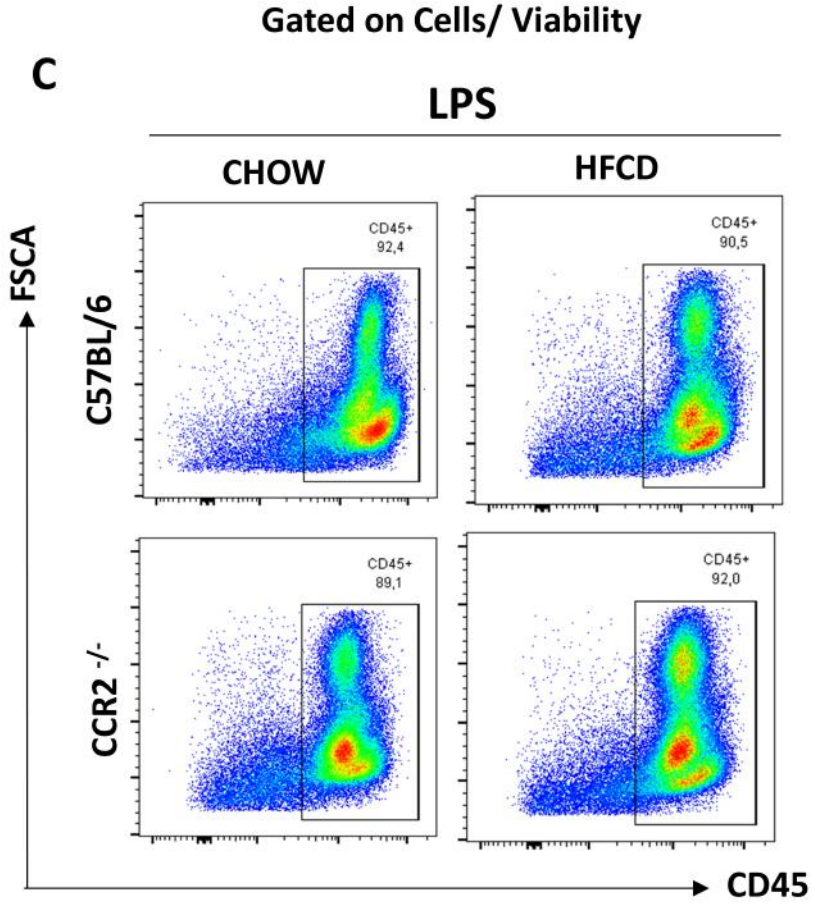

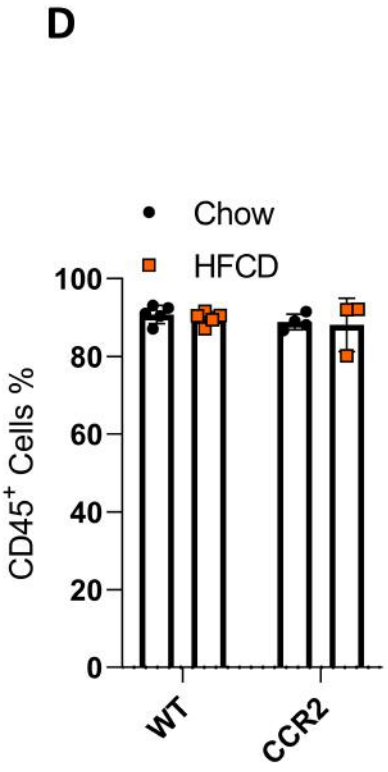

Figure S6. Neutrophils are the main PD-L1–expressing subset among CD45⁺CD11b⁺ leukocytes

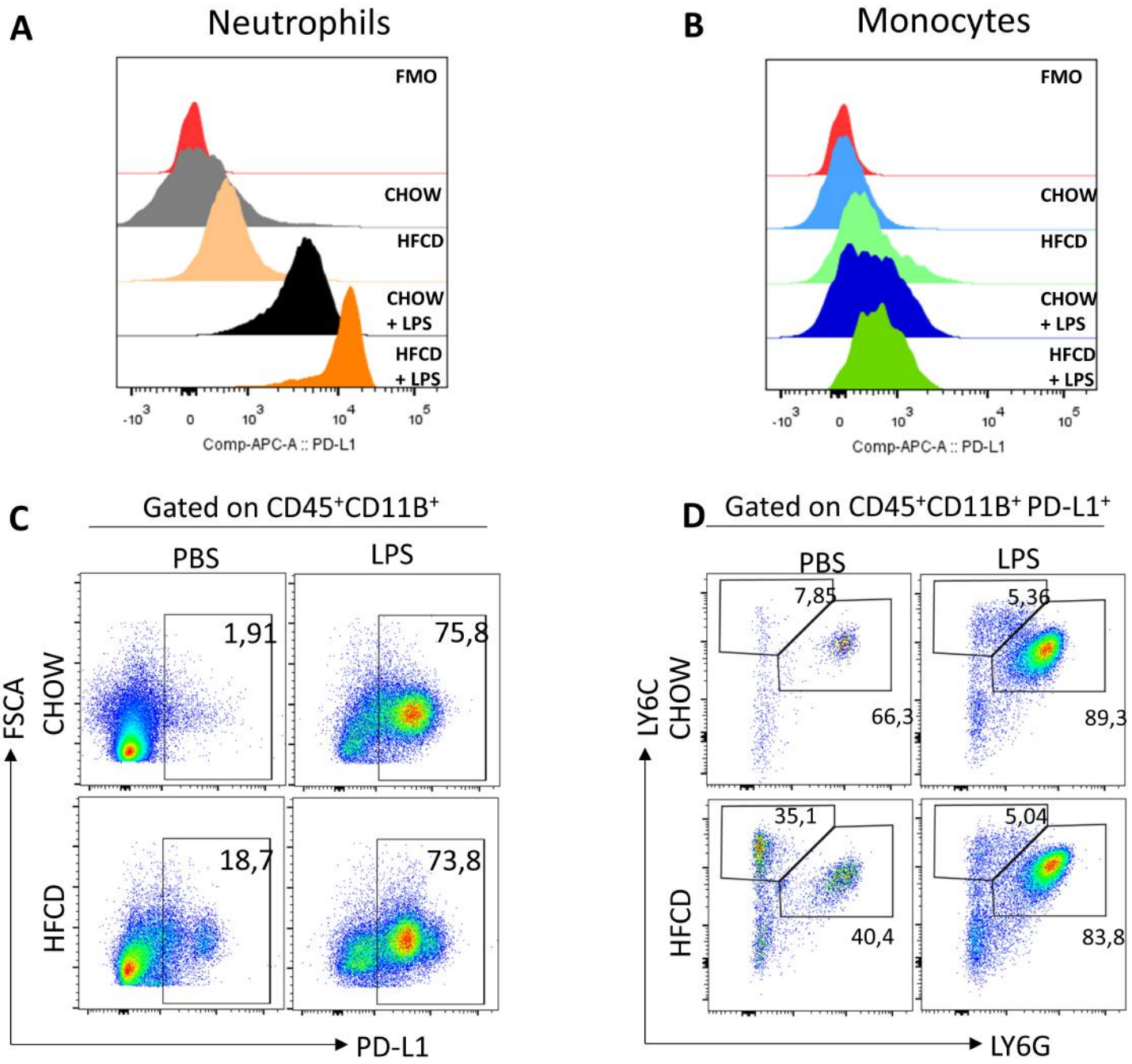

Figure S7. CXCR2i treatments reduce IFN-γ in liver tissue in animals with MAFLD to endotoxemia

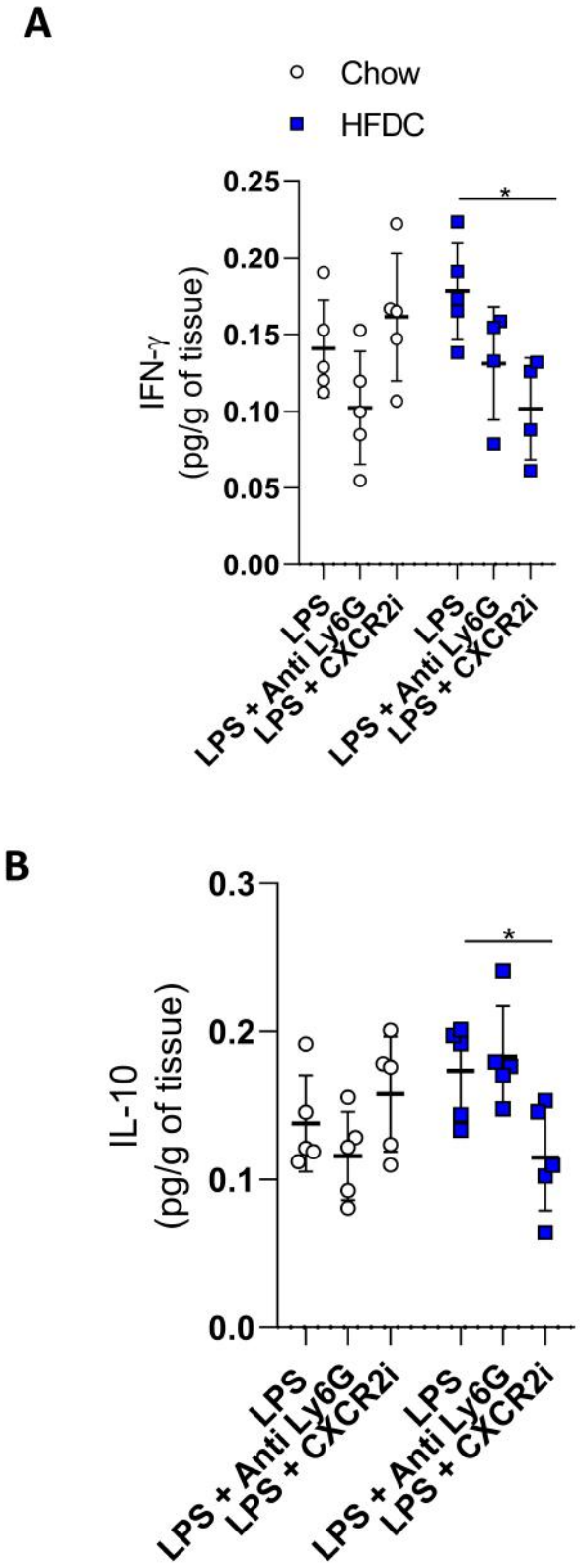

Figure S8. TNFR1/R2 $^{-/-}$ animals not have reduced neutrophil infiltration in the hepatic tissue of animals with MAFLD during endotoxemia

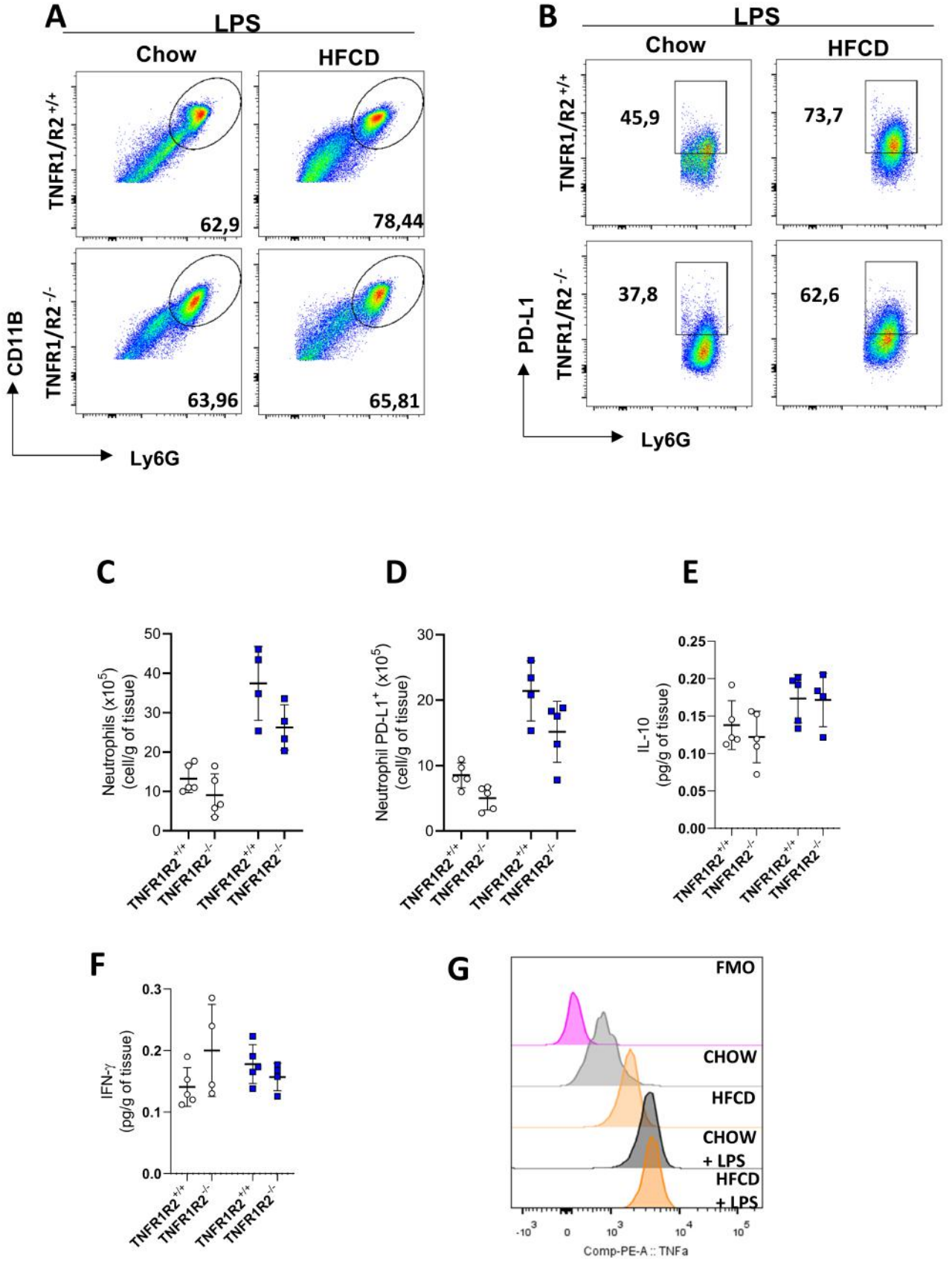

Figure S9. PD-L1 expression in neutrophils occurs in the liver and not in the lung in animals with MAFLD during endotoxemia

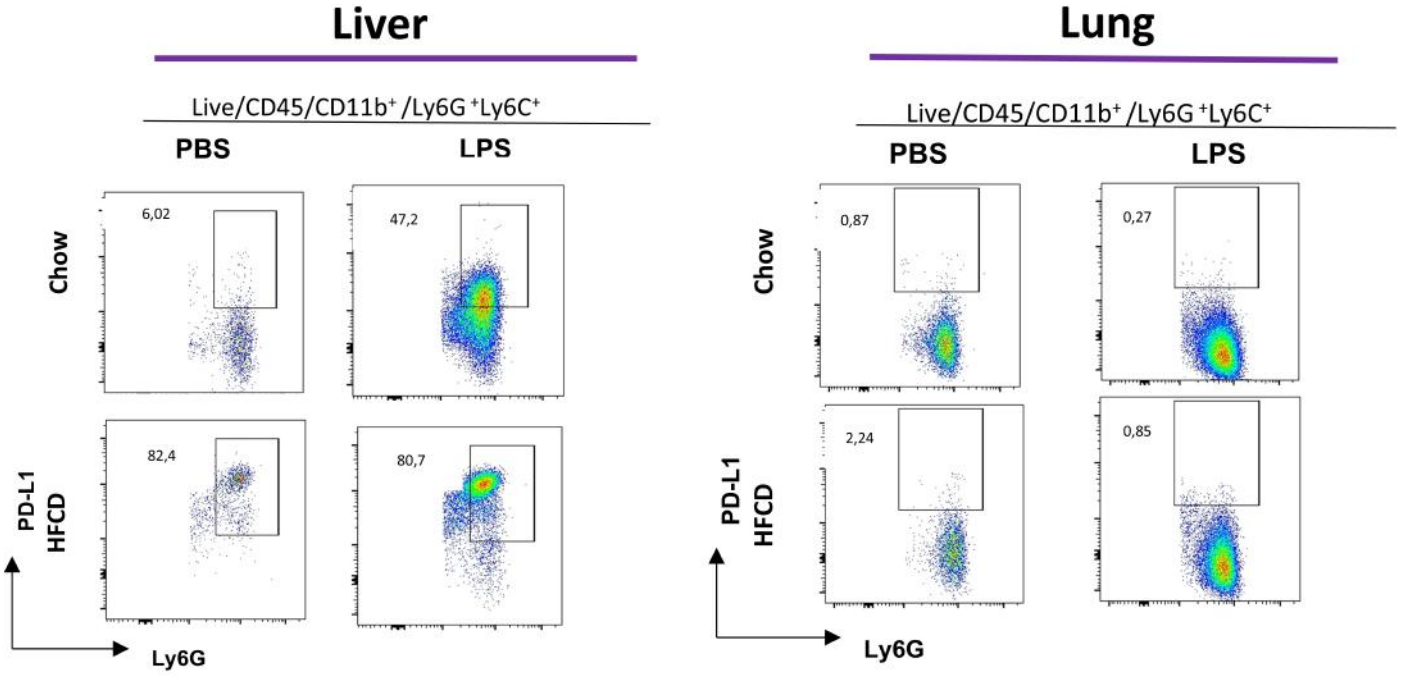

Figure S10. Gating strategy for identification of NK, CD4 and CD8 T cells

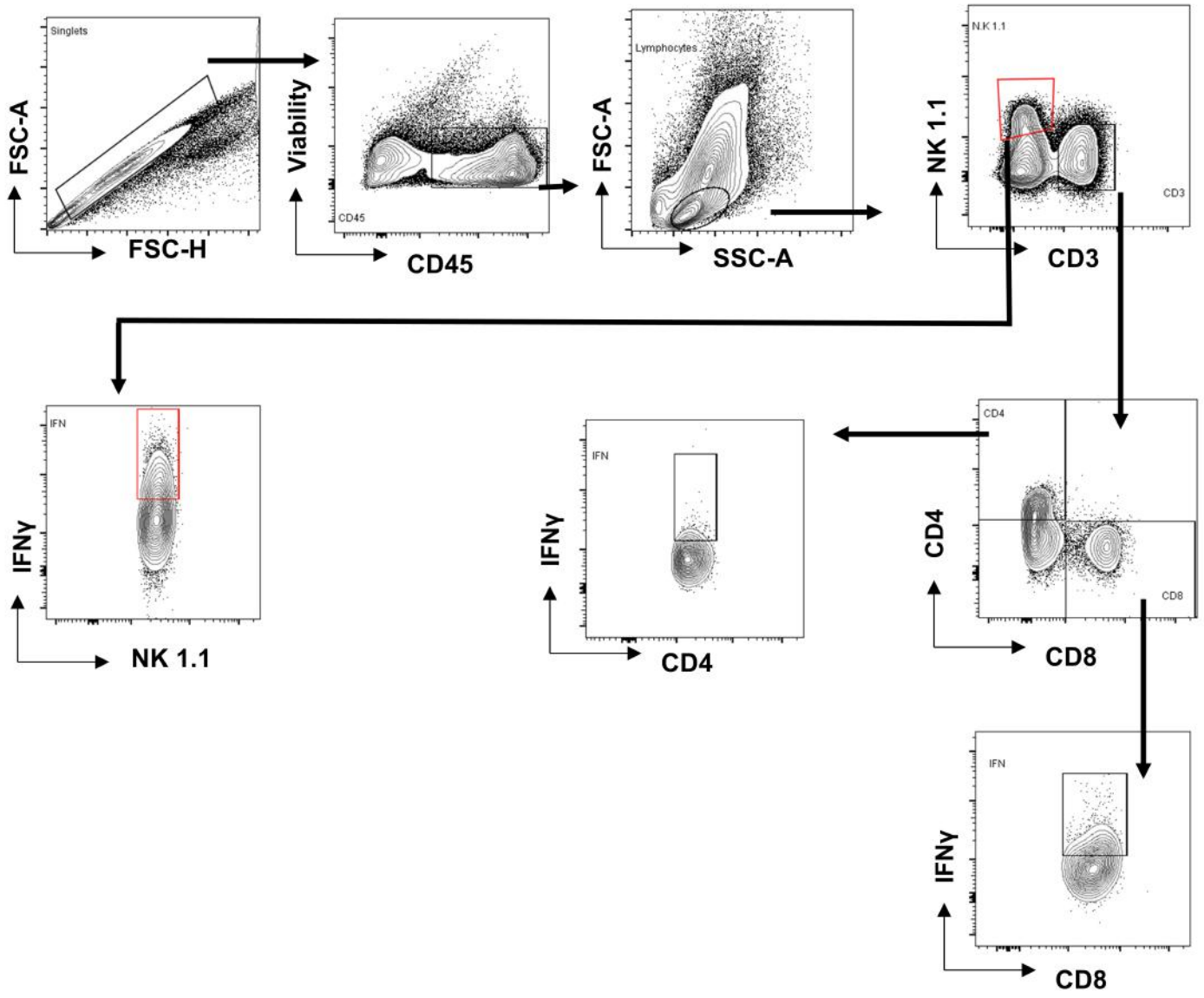
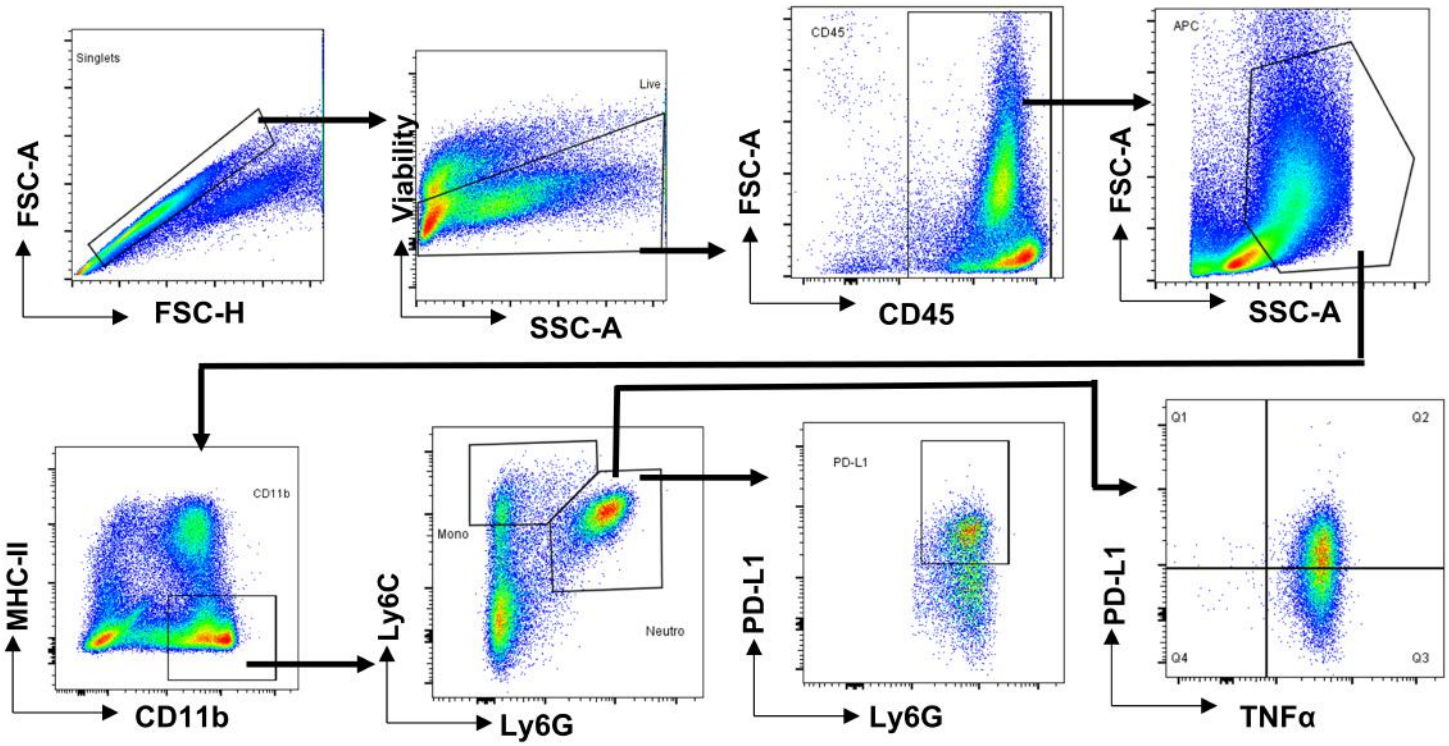
Figure S11. Gating strategy for identification of PD-L1+ neutrophils